iScience

CellPress
OPEN ACCESS

Article

Airway microbiome signature accurately discriminates *Mycobacterium tuberculosis* infection status

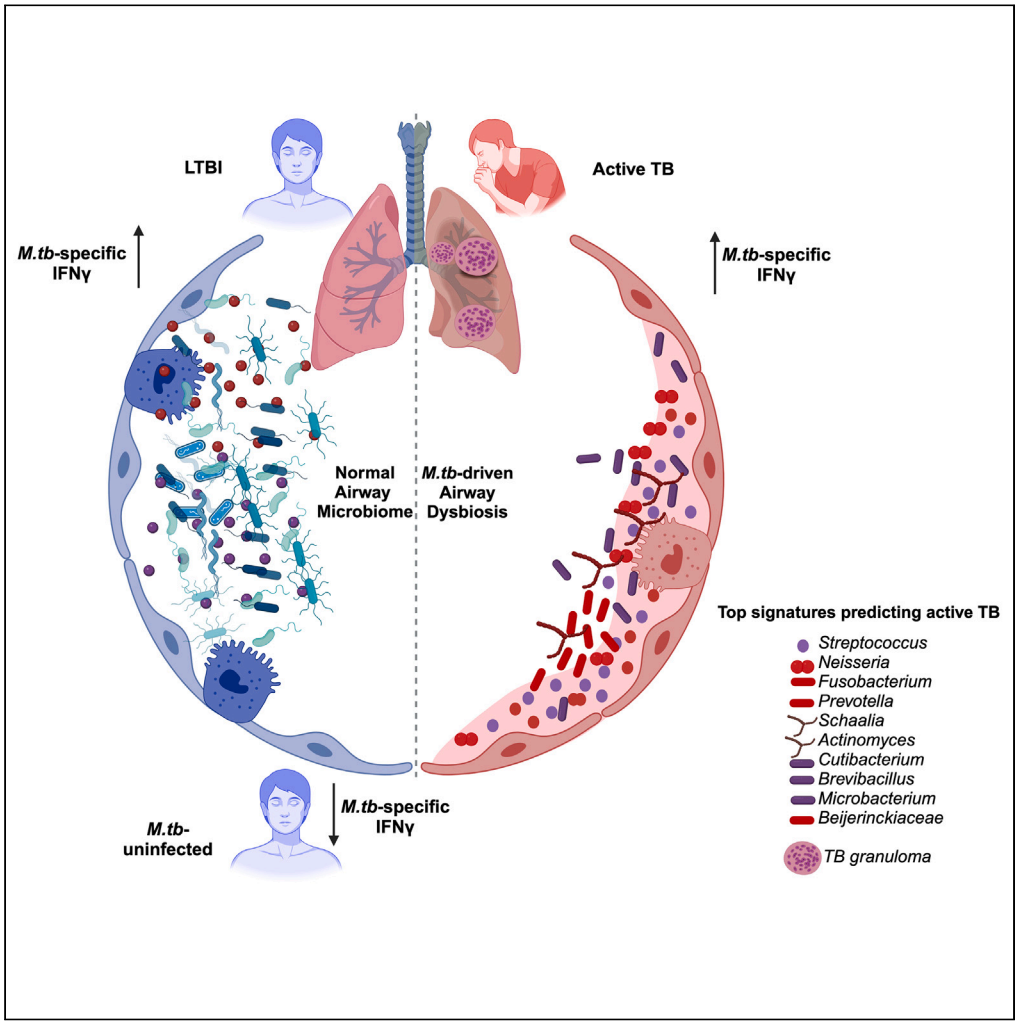

Alex Kayongo, Moses Levi Ntayi, Geoffrey Olweny, ..., Daudi Jjingo, Obondo James Sande, Harriet Mayanja-Kizza

akayongo@chs.mak.ac.ug

Highlights

M.tb infection drives a significant reduction in airway microbiome diversity

M.tb-specific IFNg does not directly impact airway microbiome diversity

Airway microbiome signature discriminates active TB from LTBI and uninfected states

LTBI and *M.tb*-uninfected states display similar airway microbiome diversity

Kayongo et al., iScience *27*, 110142
June 21, 2024
https://doi.org/10.1016/j.isci.2024.110142

iScience

CellPress
OPEN ACCESS

Article

Airway microbiome signature accurately discriminates *Mycobacterium tuberculosis* infection status

Alex Kayongo,[1,2,7,9,*] Moses Levi Ntayi,[1,2,7] Geoffrey Olweny,[1,7] Edward Kyalo,[1,2] Josephine Ndawula,[1,2] Willy Ssengooba,[1,2] Edgar Kigozi,[1] Robert Kalyesubula,[3,4] Richard Munana,[3] Jesca Namaganda,[1,2] Musiime Caroline,[1] Rogers Sekibira,[1] Bernard Sentalo Bagaya,[1] David Patrick Kateete,[1] Moses Lutaakome Joloba,[1] Daudi Jjingo,[5,6] Obondo James Sande,[1,8] and Harriet Mayanja-Kizza[4,8]

SUMMARY

***Mycobacterium tuberculosis* remains one of the deadliest infectious agents globally. Amidst efforts to control TB, long treatment duration, drug toxicity, and resistance underscore the need for novel therapeutic strategies. Despite advances in understanding the interplay between microbiome and disease in humans, the specific role of the microbiome in predicting disease susceptibility and discriminating infection status in tuberculosis still needs to be fully investigated. We investigated the impact of *M.tb* infection and *M.tb*-specific IFNγ immune responses on airway microbiome diversity by performing TB GeneXpert and QuantiFERON-GOLD assays during the follow-up phase of a longitudinal HIV-Lung Microbiome cohort of individuals recruited from two large independent cohorts in rural Uganda. *M.tb* rather than IFNγ immune response mainly drove a significant reduction in airway microbiome diversity. A microbiome signature comprising *Streptococcus, Neisseria, Fusobacterium, Prevotella, Schaalia, Actinomyces, Cutibacterium, Brevibacillus, Microbacterium,* and *Beijerinckiacea* accurately discriminated active TB from Latent TB and *M.tb*-uninfected individuals.**

INTRODUCTION

Despite the availability of effective anti-tubercular drugs and BCG vaccine, *Mycobacterium tuberculosis* (*M.tb*) remains one of the most deadly infectious agents globally.[1] Amidst efforts to control tuberculosis disease, challenges such as long treatment duration, drug toxicity, and resistance underscore the need for novel therapeutic strategies.[2,3] In addition, the poorly characterized immune mechanisms of anti-*M.tb* host defense challenges the development of robust host-directed therapeutic strategies. Tuberculin skin test and interferon-gamma release assay (IGRA) have been commonly used to test for prior *M.tb* exposure. Following exposure to aerosols contaminated with *M.tb*, 90% of infected individuals remain asymptomatic, TST and IGRA-positive, commonly referred to as latent TB infection (LTBI), whereas about 5–10% develop progressive tuberculosis disease (active TB disease).[4]

Despite advances in understanding the interplay between microbiome and disease in humans, the specific role of the microbiome in predicting disease susceptibility as well as discriminating infection status in tuberculosis still needs to be fully investigated. Some studies provide preliminary findings that warrant further investigation. Mice colonized with *Helicobacter hepaticus*, show poor *M.tb* control after an aerosol challenge with a virulent *M.tb* strain,[5] characterized by heightened airway inflammation and severe lung pathology.[6] *Helicobacter pylori* has also been implicated in tuberculosis. Macaques challenged with *M.tb* are less likely to progress to active tuberculosis disease if infected with *Helicobacter pylori*. Besides *Helicobacter* species, additional studies suggest that altering the microbiome could improve tuberculosis outcomes. Administration of *Mycobacterium manresensis* to mice undergoing *M.tb* treatment results in a more significant reduction in the airway bacillary load, pro-inflammatory cytokines, and a reduction in granuloma formation. Furthermore, the *Clostridium*-derived metabolite indole-propionic acid restricts *M.tb* growth at physiological concentrations and could be critical in *M.tb* control.[7,8] Indeed, a reduction in the

[1]Department of Immunology and Molecular Biology, Makerere University, College of Health Sciences, Kampala 256, Uganda
[2]Lung Institute, Makerere University College of Health Sciences, Kampala 256, Uganda
[3]Department of Research, African Community Center for Social Sustainability (ACCESS), Nakaseke 256, Uganda
[4]Department of Medicine, Makerere University, College of Health Sciences, Kampala 256, Uganda
[5]College of Computing and Information Sciences, Computer Science, Makerere University, Kampala 256, Uganda
[6]African Center of Excellence in Bioinformatics and Data Science, Infectious Diseases Institute, Kampala 256, Uganda
[7]These authors contributed equally
[8]Senior authors
[9]Lead contact
*Correspondence: akayongo@chs.mak.ac.ug
https://doi.org/10.1016/j.isci.2024.110142

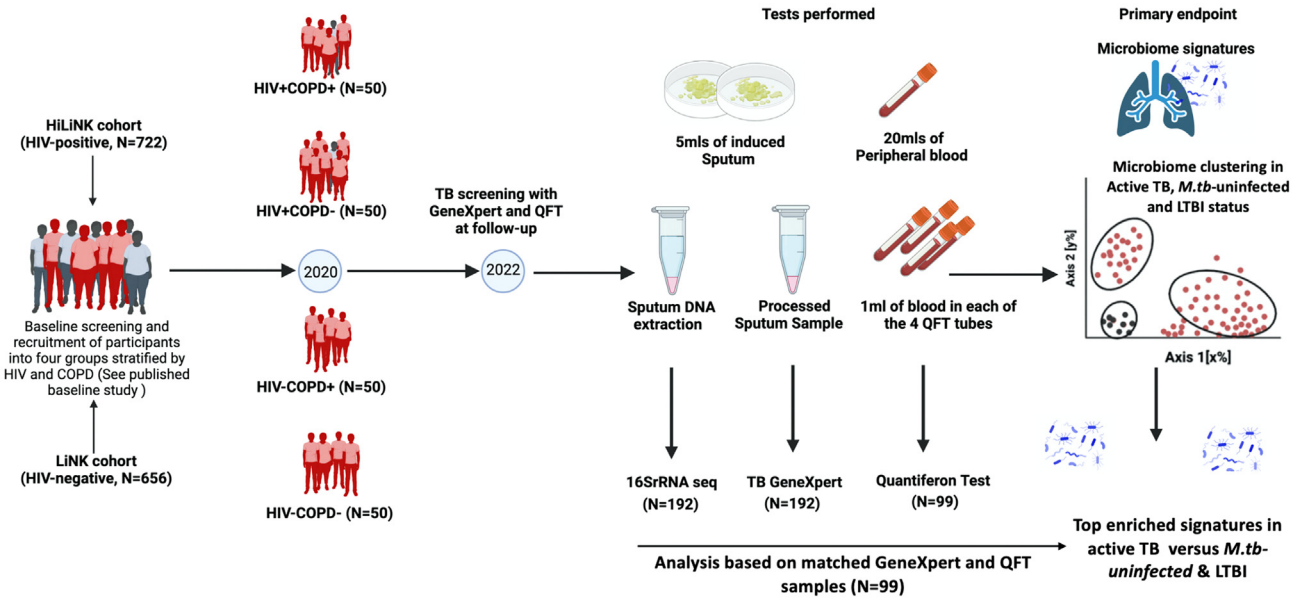

Figure 1. Study design schema

Two hundred (200) participants from two large independent cohorts in rural Uganda (LiNK/HiLiNK) were recruited into COPD-HIV-, COPD-HIV+, COPD+HIV-, COPD+HIV+ groups underwent sputum induction and TB screening using GeneXpert (N = 192) and QFT(N = 99) at follow-up. 16S sequence analysis and signature clustering based on matched GeneXpert and QFT samples (N = 99) were successfully completed to underpin top microbiome signatures enriched in active TB, LTBI, and *M.tb*-uninfected individuals.

microbiome diversity following antibiotic therapy is associated with high *M.tb* burden and severe mucosal pathology, whose rescue happens following a fecal transplant from untreated control mice.[9] Significantly, the immune profile is also restored with a reduction in regulatory T-cells and a proportionate increase in IFNγ and TNF-α.[9] Despite this evidence, further investigation is, however, warranted to determine mechanistically how microbiome signatures predict tuberculosis disease susceptibility and/or discriminate *M.tb* infection status.

Significant changes in the microbiome occur in the setting of tuberculosis. Individuals with tuberculosis are enriched with short-chain fatty acid-producing bacteria, *Roseburia* and *Faecalibacterium* spp, and are depleted for *Prevotella*.[10,11] As described by several authors, short-chain fatty acids (SCFAs) induce anti-inflammatory, tolerogenic immune responses that dampen anti-*M.tb* immunity.[12,13] Enrichment with *Streptococcus and Neisseria* and a reduction in *Prevotella* spp *have* been reported in tuberculosis.[14,15] In a meta-analysis, *Rothia, Actinomyces, Campylobacter,* and *Solobacterium* clustered with *M.tb*.[16] In another study that used bronchoalveolar lavage samples, *M.tb* and *Porphyromonas* spp were enriched in the diseased.[17] In the HIV setting, studies report enrichment with *Prevotella* and high levels of serum SCFAs, correlating with high regulatory T-cells.[18] Furthermore, increasing levels of SCFAs predicted incident tuberculosis. Strikingly, butyrate induced robust IFNγ and IL-17A production in peripheral blood mononuclear cells stimulated *ex vivo* with *M.tb*.[18] Significant changes in the airway microbiome have also been induced by *anti-M.tb* drugs,[19–21] although recent studies report restoration of the airway microbiome following successful treatment with anti-*M.tb* drugs.[22–24]

Despite this evidence, several questions remain unanswered. Does the airway microbiome influence *M.tb*-specific immune response? Is there any immune-modulatory role played by the airway microbiome in *M.tb*-induced immune response? Do specific microbiome signatures predict infection status? How the immune response is modulated to predict progression also remains to be investigated. To the best of our literature search, evidence supporting the role of the airway microbiome in moderating *M.tb*-specific immune response is very limited. In this study, we aimed to determine the airway microbiome signatures associated with *M.tb* burden and *M.tb*-specific IFNγ responses and underpin a microbiome signature that accurately discriminates *M.tb* infection status in an Ugandan cohort. Identification of novel signatures as microbiome biomarkers for discriminating *M.tb* infection status has not yet been realized, an effort which could improve TB diagnostics especially in the difficult-to-diagnose TB cases.

RESULTS

M.tb-specific IFNγ profile of a rural Ugandan cohort shows a comparable prevalence between positive and negative IFNγ responders

To determine *M.tb*-specific IFNγ immune responses and *M.tb*-burden in a rural Ugandan cohort, we screened for TB using QuantiFERON (QFT) and GeneXpert (Xpert) assays during the follow-up phase of a longitudinal HIV-Lung Microbiome cohort assembled from two large independent cohorts (i.e., *Lung Function in Nakaseke and Kampala study* (LiNK, n = 656 participants)[25] and *HIV-infected Lung Function in Nakaseke study* (HiLiNK, n = 722)[26] in the same geographic location. Figure 1 summarizes participant screening and enrollment. Overall,

Table 1. Sociodemographic and clinical characteristics of study participants

Characteristics	QFT+/Xpert+ (Active TB, *N* = 32) (%) n	QFT+/Xpert- (LTBI, *N* = 21) (%) n	QFT-/Xpert- (*M.tb*-uninfected, *N* = 46) n(%)	[a]*p* value (x^2)
Sex				
Female	38% (12)	33% (7)	33% (15)	<0.001
Male	62% (20)	67% (14)	67% (31)	<0.001
Age group (years)				
35–39	100% (32)	0% (0)	0% (0)	<0.001
40–44	0% (0)	0% (0)	9% (4)	
45–54	0% (0)	29% (6)	28% (13)	
55+	0% (0)	71% (15)	63% (29)	
HIV status				
Positive	59% (19)	33% (7)	57% (27)	<0.001
Negative	41% (13)	67% (14)	43% (19)	<0.001
CD4 count if HIV+ve				
<200	0% (0)	0% (0)	0% (0)	
200-<500	5% (14)	0% (0)	0% (0)	0.08
>500	95% (18)	100% (21)	100% (27)	<0.001
ART				
Yes	100% (32)	86% (18)	52% (14)	<0.001
No	0% (0)	14% (3)	48% (13)	
HIV viral load				
<20 copies/mL	100% (32)	86% (18)	100% (27)	<0.001
>20 copies/mL	0% (0)	14% (3)	0% (0)	
Septrin use				
Yes	0% (0)	14% (0)	14% (0)	
No	100% (32)	100% (21)	100% (27)	
COPD diagnosis				
Yes	100% (32)	29% (6)	52% (24)	<0.001
No	0% (0)	71% (15)	48% (22)	
COPD treatment				
Prednisolone	0% (0)	0% (0)	4% (2)	
Salbutamol	0% (0)	5% (21)	0% (0)	
TB treatment				
Yes	0% (0)	0% (0)	0% (0)	
No	100% (32)	100% (21)	100% (46)	
BMI categories (kg/m^2)				
<18.5	81% (26)	14% (3)	28% (13)	<0.001
18.5–24.9	19% (6)	67% (14)	63% (29)	<0.001
25.0–29.9	0% (0)	19% (4)	14% (0)	
30.0+	0% (0)	0% (0)	9% (4)	
Smoking history				
Non-smoker	100% (32)	76% (16)	54% (25)	<0.001
Daily smoker	0% (0)	10% (2)	30% (14)	

(*Continued on next page*)

Table 1. *Continued*

Characteristics	QFT+/Xpert+ (Active TB, *N* = 32) (%) n	QFT+/Xpert- (LTBI, *N* = 21) (%) n	QFT-/Xpert- (*M.tb*-uninfected, *N* = 46) n(%)	[a]*p* value (x^2)
Occasional smoker	0% (0)	14% (3)	16% (7)	
Respiratory symptoms				
Cough	100% (32)	0% (0)	4% (2)	**<0.001**
Phlegm	100% (32)	0% (0)	7% (3)	**<0.001**
Shortness of breath	100% (32)	29% (21)	52% (24)	**<0.001**

[a]Chi-squared test was used and alpha was set at 0.05.

54% (53/99) of participants had a positive QFT with a mean IFNγ response of 6.27 (95% CI: 5.14–7.38) and 6.04 (95% CI: 4.90–7.17) IU/mL to *M.tb*-specific antigens TB1 and TB2 respectively. Comparably, about 46% (46/99) of participants had a negative QFT with a mean IFNγ response of 0.08 (95% CI: 0.04–0.12) and 0.1 (95% CI: 0.06–0.14) IU/mL to TB1 and TB2 respectively. QFT-positivity showed a bimodal distribution with age, peaking in the age brackets <40 years and >55 years ($p < 0.001$). HIV status (p=0.663) and sex ($p = 0.445$) did not significantly affect QFT status. Table 1 summarises the sociodemographic and clinical characteristics of the study population, stratified as active TB disease (QFT+/Xpert+) with 32 individuals, Latent TB infection, LTBI (QFT+/Xpert-) with 21 individuals, and *M.tb*-uninfected (QFT-/Xpert-) with 46 individuals. Active TB participants were predominantly male ($p < 0.001$), between 35 and 39 years ($p < 0.001$), predominantly HIV-seropositive ($p < 0.001$), well-controlled on ART with CD4+T cell count above 500 ($p < 0.001$) and undetectable HIV viral load ($p < 0.001$). All active TB participants had COPD ($p < 0.001$), no history of prednisone or salbutamol use, and had not yet started anti-TB treatment by the time of screening. These individuals had a low body mass index ($p < 0.001$) and reported respiratory symptoms of chronic cough, phlegm, and difficulty in breathing ($p < 0.001$). LTBI participants were predominantly male ($p < 0.001$), above 55 years of age ($p < 0.001$), predominantly HIV sero-negative ($p < 0.001$), with a low COPD prevalence ($p < 0.001$), non-smoker with a normal body mass index ($p < 0.001$). LTBI participants with COPD reported shortness of breath($p < 0.001$). The *M.tb*-uninfected group were predominantly male ($p < 0.001$), above 45 years of age ($p < 0.001$), predominantly HIV sero-positive ($p < 0.001$), well controlled on ART with CD4+T cell count above 500 ($p < 0.001$) and undetectable HIV viral load ($p < 0.001$). COPD-positive and negative individuals were comparable in this group, with COPD cases predominantly reporting shortness of breath. The group was predominantly non-smoker with a normal body mass index ($p < 0.001$). In conclusion, the *M.tb*-specific IFNγ profile of a rural Ugandan cohort shows a comparable prevalence between positive and negative IFNγ responders.

Changes in the airway microbiome are mainly driven by *M.tb* rather than IFNγ immune responses in a rural Ugandan Cohort

To investigate the relationship between airway microbiome composition, *M.tb* burden and *M.tb*-specific IFNγ immune responses in a rural Ugandan cohort, we performed 16SrRNA amplicon sequencing on induced sputum samples to determine the airway microbiome profile as our primary endpoint. We explored the airway microbiome compositional differences across the three strata, i.e., *M.tb*-uninfected, LTBI, and active TB at phylum (Figure 2A) and genus level (Figure 2B). Overall, at the phylum level, airways were enriched for *Firmicutes, Actinobacteriota, Proteobacteria, Bacteroidota, Fusobacteriota, Patescibacteria, Campylobacteriota, Spirochaetota, and Verrucomicrobiota.* The phyla *Firmicutes* (∼50%), *Proteobacteria* (∼20%), *Bacteroidota* (∼20%), *and Fusobacteriota* (<10%) significantly enriched the airways of *M.tb*-uninfected. As expected, Active TB samples were significantly enriched for *Actinobacteriota* (>90%) and depleted for *Firmicutes* (<10%), *Proteobacteria* (<5%), and *Bacteroidota* (<1%), while *M.tb*-uninfected and LTBI samples were significantly enriched for *Firmicutes* (∼50%), *Proteobacteria* (∼20%) and *Bacteroidota* (∼20%) and depleted for *Actinobacteriota* (<10%). There was no significant difference in the composition of the airway microbiome between *M.tb*-uninfected and LTBI samples. At the genus level, active TB airway samples were enriched for *Mycobacterium* (∼80%), *Streptococcus* (∼10%), *Brevibacillus* (∼10%), *Streptomyces* (∼5%) and depleted for *Stenotrophomonas* (<1%), *Fusobacterium* (<1%), *Neisseria* (<1%), *Prevotella* (<1%) and Veillonella (<1%). *M.tb*-uninfected and LTBI samples were comparably enriched for *Streptococcus* (>40%), *Prevotella* (>10%), *Neisseria* (>5%), *Fusobacterium* (>5%), *Stenotrophomonas* (>5%) and *Veillonella* (>5%).

Based on these findings, we further investigated the relationship between *M.tb*-specific IFNγ responses and airway microbiome composition. We computed the metrics of microbiome diversity within samples (alpha diversity scores) and between samples (beta diversity). First, we compared alpha diversity indices across the three strata (Figure 2C). We observed a significant reduction in microbial richness based on Shannon, Chao1, and the Observed number of genera among active TB compared to *M.tb*-uninfected and LTBI individuals (Wilcoxon test, $p < 0.0001$). Furthermore, airway microbial evenness based on Pielou, Simpson, and Inverse Simpson scores was significantly decreased among active TB compared to *M.tb*-uninfected and LTBI individuals (Wilcoxon test, $p < 0.0001$). While we observe a significant difference in both richness and evenness indices between active TB versus *M.tb*-uninfected and LTBI individuals, it is comparable between uninfected and LTBI individuals. We projected the genus-level airway microbiome composition of all samples according to the three strata and performed Principal coordinates (PCoA) analysis of the Bray–Curtis dissimilarity of induced sputum samples (Figure 2D). Samples separated into two distinct clusters i.e., *M.tb*-uninfected and LTBI versus active TB disease. To confirm whether the observed changes in airway microbiome were mainly driven by *M.tb* rather than IFNγ immune responses, we analyzed alpha diversity based on of TB GeneXpert status alone. A significant reduction in bacterial richness based on Shannon, Observed, and Chao 1 indices, as well as evenness based on Pielou, Simpson,

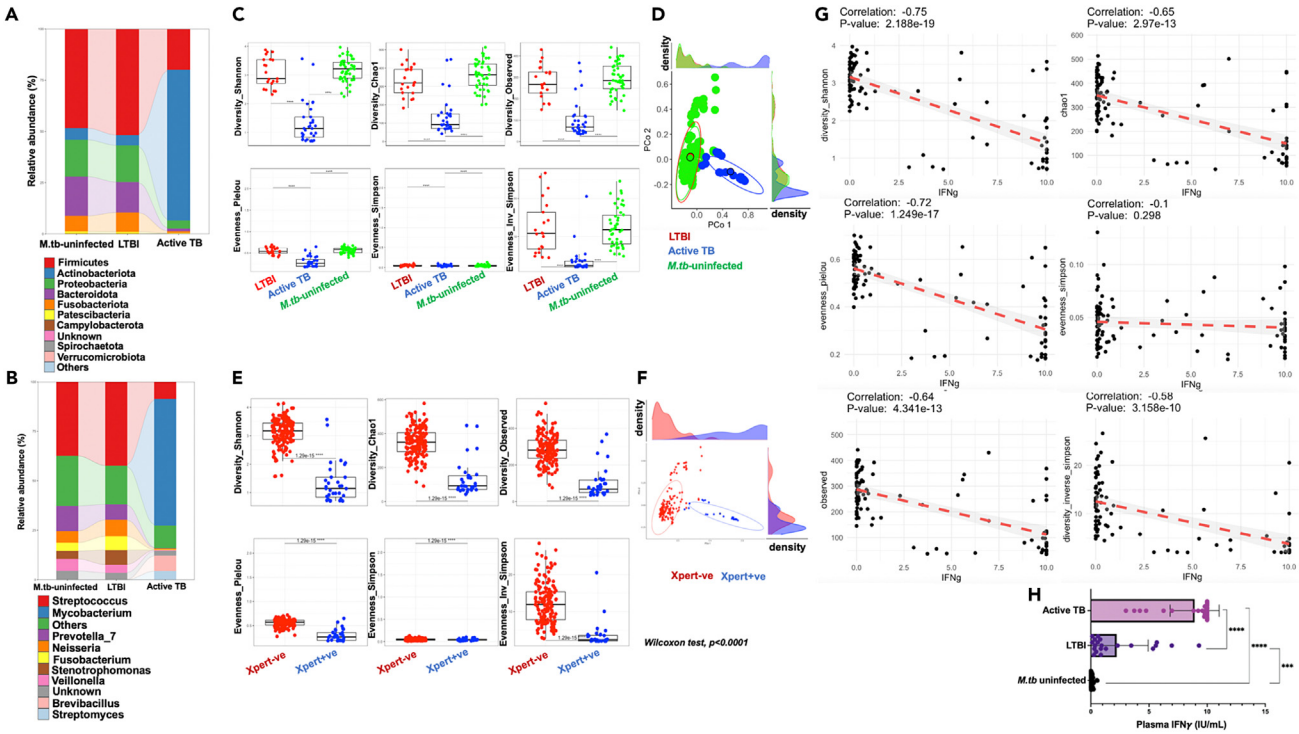

Figure 2. Changes in the airway microbiome are mainly driven by *M.tb* rather than IFNγ immune responses in a rural Ugandan Cohort

Bar plots showing the percentage relative abundance of the sputum operational taxonomical units (OTUs) at phylum (A) and genus (B) level across three strata: Active TB, LTBI, and *M.tb*-uninfected group.

(C) Boxplots showing the alpha diversity indices for richness (Shannon, Chao and observed number of genera) and evenness (Pielou, Simpson and Inverse Simpson) per Active TB, LTBI and M.tb-uninfected strata. A pairwise Wilcoxon test corrected for multiple testing using a False Discovery Rate was performed.

(D) Principal coordinates analysis (PCoA) plots of Bray Curtis dissimilarity of sputum samples stratified by active TB, LTBI, and *M.tb*-uninfected status. Marginal density plots depict sample group distribution alongside PCo1 and PCo2. Ellipses represent the 95% confidence interval for each cluster.

(E) Boxplots showing the alpha diversity indices for richness (Shannon, Chao and observed number of genera) and evenness (Pielou, Simpson and Inverse Simpson) per GeneXpert positive versus negative. A pairwise Wilcoxon test using a False Discovery Rate was performed.

(F) Principal coordinates analysis (PCoA) plots of Bray Curtis dissimilarity of sputum samples stratified by GeneXpert positive versus negative status. Marginal density plots depict sample group distribution alongside PCo1 and PCo2. Ellipses represent the 95% confidence interval for each cluster.

(G) Scatterplots for diversity indices of richness (Shannon, Chao, and observed number of genera) and evenness (Pielou, Simpson, and Inverse Simpson) with *M.tb*-specific IFNγ responses. Shown are Spearman's rho, *p*-values, and the 95% confidential interval. Spearman's rank correlation coefficient was performed.

(H) Bar plots showing plasma *M.tb*-specific IFNγ per active TB ($n = 32$), LTBI ($n = 21$) and *M.tb*-uninfected ($n = 46$) group. Mann-Whitney U test was performed and alpha set at 0.05, ****, *p*-value<0.0001.

and Inverse Simpson indices, was detected among active TB (Xpert-positive) individuals compared to the *M.tb*-uninfected and LTBI (Xpert-negative) individuals (Figure 2E). Projection of genus-level airway microbiome composition of samples according to Gene Xpert status and Principal coordinates analysis (PCoA) of Bray Curtis dissimilarity of induced sputum samples revealed a similar pattern of sample clustering (Figure 2F), confirming that *M.tb* predominantly drives changes in the airway microbiome composition. Additionally, we used Spearman's rank correlation analysis to illustrate the relationship between airway microbiome alpha diversity metrics and *M.tb*-specific IFNγ responses based on IGRA values rather than a different *M.tb*-specific IFNγ ELISA assay (Figure 2G). We observe a strong negative correlation between *M.tb*-specific IFNγ responses and microbiome richness based on Shannon, Chao1, and the Observed number of genera and evenness scores based on Pielou, Simpson and Inverse Simpson scores ($p < 0.0001$) except for Simpson's index ($p = 0.298$). The significantly high IFNγ response was driven by active TB (Figure 2H). Further comparison of microbiome diversity indices between LTBI samples with higher *M.tb*-specific IFNγ responses (2.5–7.5 IU/mL) and active TB samples with similar *M.tb*-specific IFNγ responses consistently indicated that *M.tb* predominantly drives the observed changes in the airway microbiome composition (Figures S1A and S1B). In conclusion, Active TB significantly reduces airway microbiome richness and evenness. The comparable results between LTBI and the *M.tb*-uninfected population indicate that airway microbiome changes are mainly driven by *M.tb* rather than IGRA status.

Sputum microbiome typing revealed a set of airway microbiome signatures that cluster with *M.tb*

To investigate airway microbiome signatures that cluster with *M.tb* in our cohort, we fitted a Dirichlet multinomial model on the count matrix of the genus relative abundance to classify genus abundance based on probability. The best fit of the tested data revealed three

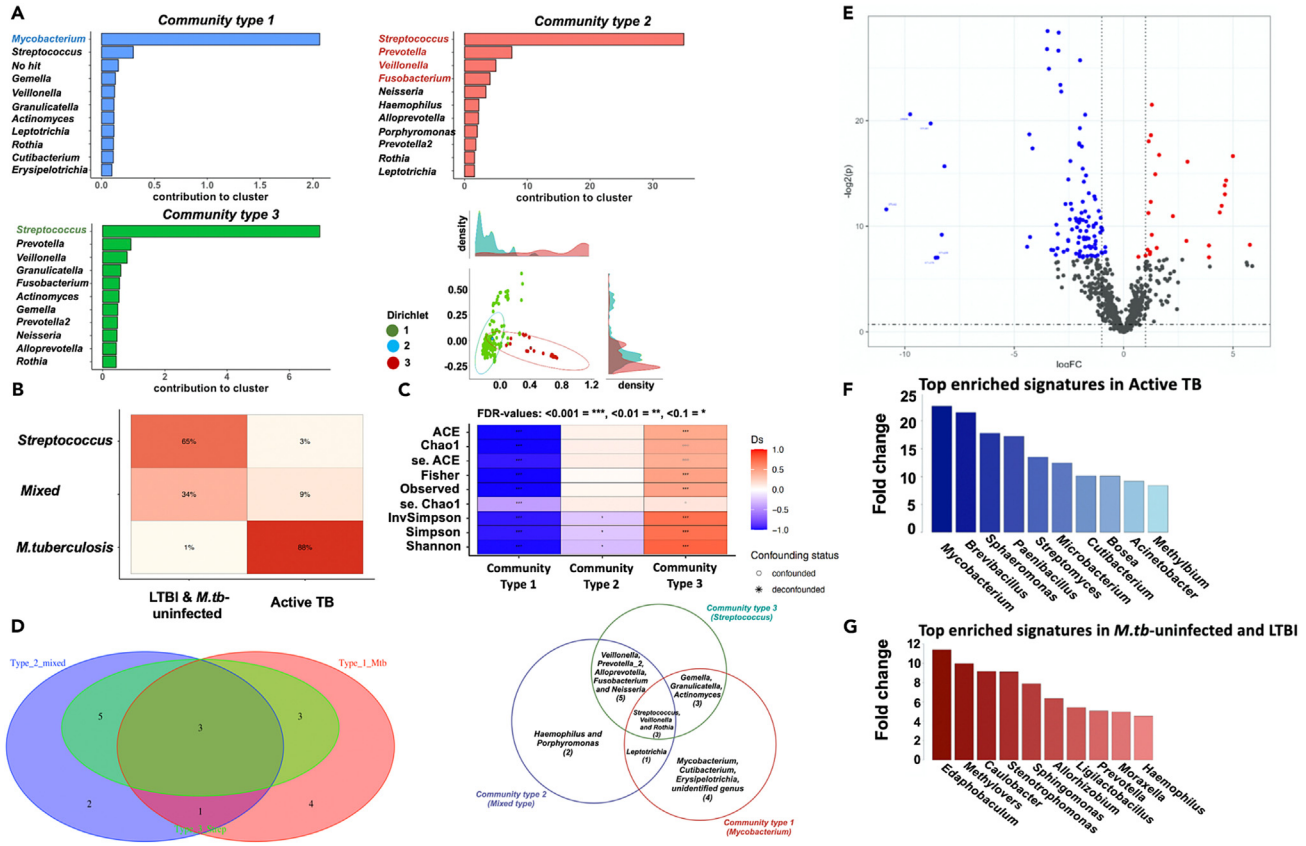

Figure 3. Sputum microbiome typing revealed a set of microbiome signatures that cluster with *M.tb*

(A) Bar plots showing the relative contribution of each operational taxonomical unit (OTU) to each community cluster. Shown in blue is the *M.tb*-dominated community type 1, red is the mixed bacterial genera community type 2, and green is the *Streptococcus*-dominated community type 3. In the lower right corner is a principal coordinates analysis (PCoA) plot of Bray Curtis dissimilarity of sputum samples stratified by community types 1, 2 and 3. Marginal density plots depict sample group distribution alongside PCo1 and PCo2. Ellipses represent the 95% confidence interval for each community cluster.

(B) A heatmap showing the distribution of community types based on active TB versus LTBI and *M.tb*-uninfected strata.

(C) A heatmap showing associations between community types and alpha indices. MetadeconfoundR was used for analysis. Cofounded results are shown with a circle, while deconfounded results are shown with a star. Cliff's delta and FRD values are shown. *** FDR<0.001, **FDR<0.01 and *FDR<0.1.

(D) Venn diagram illustrating the distribution of genera in community types 1, 2, and 3.

(E) A volcano plot showing differentially abundant airway microbiome signatures in active TB versus (blue) LTBI and *M.tb*-uninfected groups (red).

(F and G) Bar plots showing the top ten microbiome signatures enriched in active TB (shown in blue)(F) and the top ten microbiome signatures enriched in LTBI and M.tb-uninfected individuals (shown in red) (G). Analysis was performed using DeSeq and EdgeR.

Dirichlet multinomial groups, further named community types 1, 2, and 3 (Figure 3A). In community type 1, *Mycobacterium tuberculosis* clustered with *Streptococcus*, *Gemella*, *Veillonella*, *Granulicatella*, *Actinomyces*, *Leptotrichia*, *Rothia*, *Cutibacterium*, *and Erysipelotrichia*. Community type 2 had a mixed abundance of several bacterial genera, including *Neisseria*, *Streptococcus*, *Haemophilus*, *Veillonella*, *Fusobacteria*, *Porphyromonas*, *and Prevotella*, while Prevotella, Streptococcus, and Veillonella dominated community type 3. Stratification by TB status revealed significant differences in the distribution of community types. Specifically, Active TB samples were predominantly comprised of type 1 bacterial community enriched with *M.tb* (Figure 3B). A comparison of microbiome metrics of alpha diversity across the three Dirichlet multinomial groups using metadeconfoundR revealed significantly reduced bacterial richness and evenness in community type 1 compared with other community types (*FDR-value*<0.001) (Figure 3C). Using Venn diagram analysis, we carefully examined the microbial signatures to identify signatures exclusively clustering with *M.tb*. Among signatures in type 1, *Cutibacterium* and *Erysipelotrichia* uniquely clustered with *M.tb* (Figure 3D). To further underpin top microbiome signatures enriched in active TB versus *M.tb*-uninfected/LTBI individuals, we performed differential microbiome abundance analysis between active TB versus *M.tb*-uninfected and LTBI individuals, using EdgeR (3.14.0) and DESeq2 (1.43.1). We then projected the top enriched signatures in active TB versus *M.tb*-uninfected and LTBI individuals using a volcano plot (Figure 3E) and illustrated the top 10 enriched airway microbiome signatures in active TB (Figure 3F) versus *M.tb*-uninfected and LTBI groups (Figure 3G). *Mycobacterium*, *Brevibacillus, Sphaeromonas, Paenibacillus, Streptomyces, Microbacterium, Cutibacterium, Acinetobacter, and Methylbium* were enriched among the active TB group (FDR-corrected $p < 0.0001$) (Figure 3F). *Edaphobaculum, Methylovers, Caulobacter, Stenotrophomonas, Allorhizobium, ligilactobacillus, Prevotella, Moraxella, and Haemophilus* were

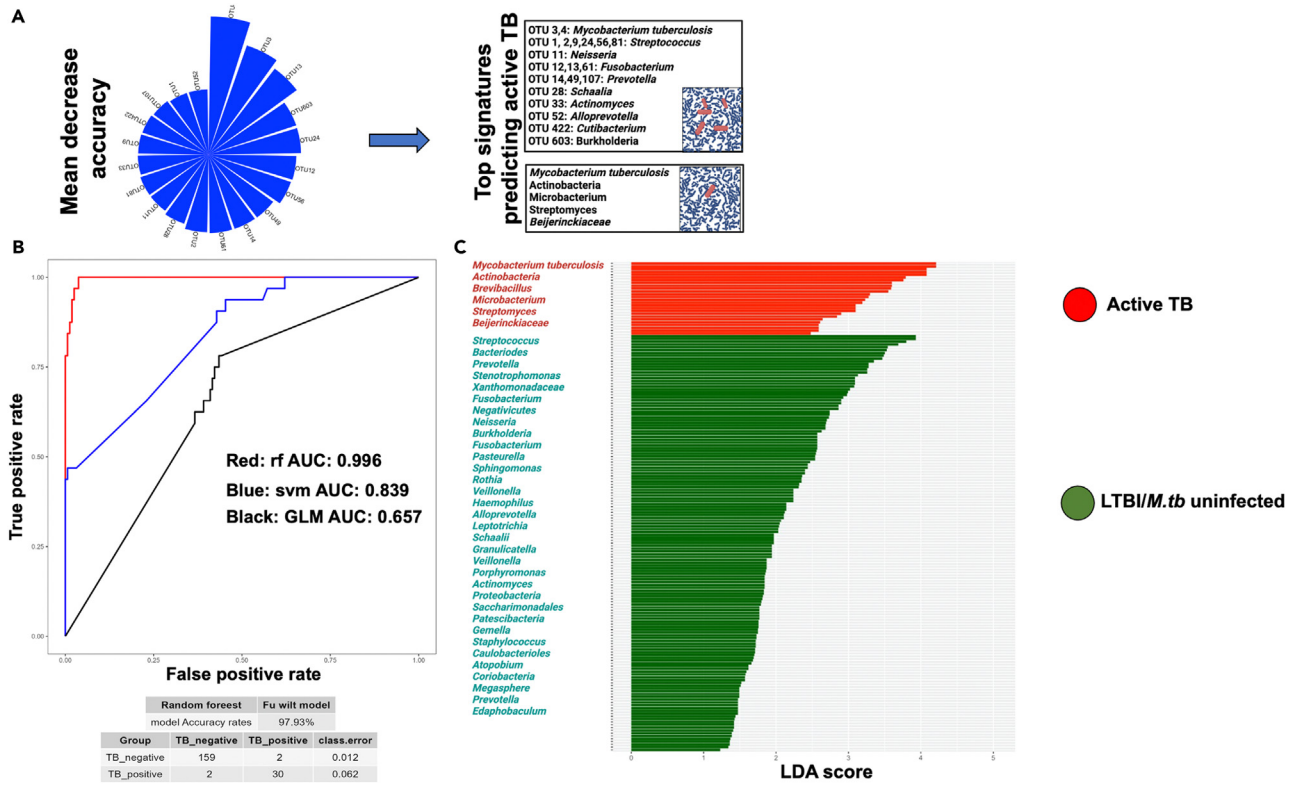

Random foreest	Fu wilt model
model Accuracy rates	97.93%

Group	TB_negative	TB_positive	class.error
TB_negative	159	2	0.012
TB_positive	2	30	0.062

Figure 4. A novel airway microbiome signature accurately discriminates *M.tb infection status*

(A) A pie chart illustrating the mean decrease accuracy values of the top airway microbiome signatures predicting active TB status compared to LTBI and *M.tb*-uninfected groups, generated using random forest analysis.

(B) Receiver operator curves (ROC) for assessing the performance of three models, i.e., the random forest model (rf, AUC = 0. 996), the support vector machine model (svm, AUC = 0. 839), and the generalized linear model (glm, AUC = 0.657). Shown at the bottom is a random forest model accuracy of 97.3%.

(C) Bar plots showing linear discriminant analysis (LDA) effect size scores of OTUs in active TB versus LTBI and M.tb-uninfected groups.

enriched among *M.tb*-uninfected and LTBI groups (FDR-corrected $p < 0.0001$) (Figure 3G). To determine the interaction networks in *M.tb*-associated airway microbiome clusters, we performed a microbial co-occurrence network analysis using Spearman's rank correlation analysis across multiple samples per TB status. Among active TB samples, the co-occurrence network analysis at the phylum level revealed three major hubs, driven by *M.tb* from *Actinobacteriota* (Figures S2A and S2B). At the genus level, *active TB* strongly correlated with *Streptococcus, Brevibacillus, Streptomyces, Bosea, Beijerinckiacea, Gemella, Alloprevotella, Sphaeriminospora, Granulicatella, Neisseria and Rothia* (Figures S2C–S2E). Co-occurrence network analysis revealed a novel airway microbiome signature as a potential biomarker that could be used to discriminate between active TB from *M.tb*-uninfected and LTBI individuals, especially in difficult-to-diagnose TB cases, or monitor treatment response among TB cases.

A novel airway microbiome signature set accurately discriminates *M.tb infection status*

Microbiome signatures selected through a difference analysis are often unable to determine whether they represent the main differences of concern or background noise as signatures. Therefore, we used machine learning and weight analysis methods to underpin signatures as potential biomarkers accurately. We used random forest analysis as a machine learning method to distinguish microbiome signatures with the potential to discriminate between active TB versus *M.tb*-uninfected and LTBI individuals. We successfully predicted an airway microbiome signature (*Streptococcus, Neisseria, Fusobacterium, Prevotella, Schaalia, Actinomyces, Alloprevotella, Cutibacterium, and Burkholderia*) as a potential biomarker for active TB (Figure 4A), using the random forest model (rf, AUC = 0. 996), the support vector machine model (svm, AUC = 0. 839) and the generalized linear model (glm, AUC = 0.657) (Figure 4B). To further confirm our biomarker prediction for active *M.tb* in our cohort, we performed Linear Discriminant Analysis Effect Size (LEfSe), a weight-based analysis method (Figure 4C). This analysis revealed that *Actinobacteria, Brevibacillus, Microbacterium, Streptomyces*, and *Beijerinckiacea* accurately discriminate active TB from *M.tb*-uninfected and LTBI individuals. In conclusion, we report a novel airway microbiome signature comprising *Streptococcus, Neisseria, Fusobacterium, Prevotella, Schaalia, Actinomyces, Cutibacterium, Brevibacillus, Microbacterium*, and *Beijerinckiacea as top predictors of active TB* in an Ugandan cohort. This signature set warrants further validation in larger TB cohorts to assess its diagnostic performance and accuracy.

COPD/HIV comorbidity does not impact the airway microbiome composition in an Ugandan rural cohort

Since a COPD/HIV cohort was used as a screening cohort for *M.tb*-associated microbiome signatures, it was critical to ascertain whether COPD/HIV comorbidity significantly impacted the airway microbiome composition. To determine the impact of HIV on airway microbiome composition, we compared alpha diversity indices between HIV-positive versus HIV-negative individuals (Figure S3A). We observed no significant differences in microbial richness based on Shannon, Chao1, and Faith's phylogenetic diversity among HIV-positive compared to HIV-negative individuals. Similarly, airway microbial evenness based on Pielou, Simpson, and Inverse Simpson scores was not significantly different among HIV-positive compared to HIV-negative individuals. We projected the genus-level airway microbiome composition of samples according to HIV status and performed Principal coordinates (PCoA) analysis of the Bray Curtis dissimilarity of induced sputum samples (Figure S3B). We observed an overlap between HIV-positive and HIV-negative samples with no significant clustering. Similarly, analysis of alpha diversity based on COPD status did not reveal any significant influence of COPD on the compositional differences of the sputum microbiota (Figure S4A). We did not observe any statistically significant difference in bacterial richness based on Shannon, Observed, and Chao 1 indices, as well as evenness based on Pielou, Simpson, and Inverse Simpson indices, between COPD-positive and COPD-negative individuals. Projection of genus-level airway microbiome composition of samples according to COPD status and Principal coordinates analysis (PCoA) of Bray Curtis dissimilarity of induced sputum samples revealed an overlap across COPD-positive and negative groups without any significant clustering (Figure S4B). To assess the impact of HIV-COPD comorbidity on airway microbiome, we compared alpha and beta diversity scores across HIV-COPD strata i.e., (COPD+/HIV+, COPD-/HIV+, COPD+/HIV-, and COPD-/HIV-) using a pairwise Wilcoxon test corrected for multiple testing. Generally, we observe homogeneity in airway microbiome diversity across COPD/HIV strata with no statistical differences (Figure S5A). This homogeneity in alpha diversity was reflected in beta diversity with significant overlap across study groups. By determining intersample Bray–Curtis dissimilarities, we summarize high-dimensional data into a reduced dimensional space to assess microbiome composition more comprehensively. Using principal coordinates analysis, the bray-Curtis dissimilarity between the different groups is visualized, with no significant differences between groups ($p > 0.05$) (Figure S5B). In conclusion, HIV and COPD comorbidities did not significantly influence the airway microbiome composition of our cohort.

DISCUSSION

In this study, we investigated the airway microbiome signature associated with *M.tb* burden and *M.tb*-specific IFNγ response and underpinned a microbiome signature that accurately discriminated active TB from LTBI and *M.tb*-uninfected individuals in a rural Ugandan cohort. *M.tb*-specific IFNγ profile of a rural Ugandan cohort showed a comparable prevalence between positive and negative IFNγ responders. Active TB significantly reduced airway microbiome richness and evenness, with comparable results between LTBI and *M.tb*-uninfected populations. These results indicated that airway microbiome changes were largely driven by *M.tb* rather than IFNγ responses. We report a novel airway microbiome signature which accurately discriminated active TB population from LTBI and *M.tb*-uninfected populations.

Whereas the prevalence of *M.tb*-specific IFNγ positive and negative immune responses was comparable in our population, IFNγ negativity was higher compared to other studies, which reported between 7% and 25% prevalence.[27–30] The interpretation of this difference in *M.tb*-specific IFNγ negativity, however, should take into account several factors, such as follow-up time, method of diagnostics such as TST and/or IGRA, degree of *M.tb* exposure, genetics, urban/rural setting, HIV status, and comorbidities.[31–33] Whereas we report a high prevalence of *M.tb*-specific IFNγ negativity at a single time-point, in longitudinal studies, we observe that the majority of individuals initially negative convert into IFNγ positive status.[33] Hence, the prevalence of *M.tb*-specific IFNγ negativity gradually declines to levels between 7 and 25%.[32,34–36] *M.tb*-specific IFNγ negativity in our study population could either mean limited exposure to index TB cases or the existence of IFNγ-independent immune responses in our study population.[32,34–36] Several social and demographic factors support the former. TB surveillance studies have reported disproportionately higher TB cases in Urban settings than in rural settings.[37] Urban settings present challenges of overcrowding in workplaces, public transportation, and living spaces compared to rural settings. Dense TB transmission networks exist in urban areas.[38,39] Regression models in TB household contact studies suggest that age, number of windows, homestead size, and sleeping in the same room are score-driving factors among individuals whose IGRA status changes from negative to positive.[31] The high *M.tb*-specific IFNγ negativity could also be accounted for by the high HIV prevalence since immunosuppression dampens T cell responses. However, well-controlled HIV with virologic suppression in our cohort underscores this possibility. We and others[40] did not report an association between HIV status and *M.tb*-specific IFNγ positivity in Uganda.

Airway microbiome interaction with *M.tb* could influence *M.tb* infection status or outcome. In this study, microbiome diversity was greatly influenced by *M.tb* infection. Moreover, active TB significantly reduced airway microbiome richness and evenness, with comparable results between LTBI and *M.tb*-uninfected populations. These results indicated that airway microbiome changes were largely driven by *M.tb* rather than IFNγ responses. The significant reduction in microbiome diversity in the context of *M.tb* infection was majorly driven by *M.tb* replication upon establishment of infection in the airways. *M.tb* infection strained the ecosystem, depleting nutrients and making it harder for symbionts to thrive and compete in the same microenvironment. Consequently, *M.tb* dominated in the airways at the expense of other bacterial species. This demonstrates cell-to-cell microbiome crosstalk that happens in the airway microenvironment.[41] *M.tb* interacts with the innate immune cells, which, upon activation, prime the adaptive system to produce type II interferons (IFNγ).[42,43] It is not surprising that IFNγ levels increased in the setting of *M.tb* and negatively correlated with airway microbiome diversity. The comparable airway microbiome profile in LTBI versus the *M.tb*-uninfected states clearly infers homogeneity in the airway microenvironment in these two states. Successful containment of the bacilli within granulomas seals off *M.tb* infection in LTBI.[44] At the airway mucosal surface, there are no significant changes in oxygen saturation and nutrient availability, which maintain cell-to-cell bacterial crosstalk.[41,45] In addition, the

proportion of keystone bacterial species is not significantly altered.[45] Therefore, a microbiome profile similar to the *M.tb*-uninfected group is maintained. What remains unknown are the acute changes in the microbiome features that signal the airway immune cells to promote *M.tb* containment. Furthermore, understanding microbiome signatures that significantly correlate with a transition from the uninfected or LTBI to active TB in a carefully designed longitudinal study will be key in understanding the critical role of the microbiome in *M.tb* infection outcomes in humans.

We successfully identified top airway microbiome signatures associated with active TB versus LTBI and *M.tb*-uninfected states using differential microbiome abundance analysis. In our study, it was evident that active TB primarily drives *M.tb*-specific IFNγ response, and its association with other bacterial genera does not directly indicate their influence on IFNγ production but rather co-existence with *M.tb*, a primary inducer of *M.tb*-specific IFNγ response. The pertinent questions to answer here are: why do such bacterial genera cluster with *M.tb* during infection, unlike other bacterial genera? Do they exert a direct immunostimulatory effect on IFNγ production? Although currently unknown, these bacterial genera might likely share a unique motif in their cell wall or produce a conserved molecule, which, upon immune recognition, can elicit or augment IFNγ responses. A detailed analysis of these signatures focusing on conserved motifs with *M.tb* is warranted. It has been recently shown that T cell immune responses can be elicited by highly expressed, widely conserved cell surface epitopes from many commensal bacteria.[46] Such motifs include specific binding protein (SBP) and tetratricopeptide repeat lipoprotein (TPRL). Furthermore, it is also likely that the metabolic needs of these genera are significantly similar to those of *M.tb* and that they co-exist in the same environment. *M.tb* most likely has a competitive advantage over the cluster of the identified bacterial genera. In the absence of *M.tb* infection, these bacteria flourish in airways with limited competition for nutrients and space.[45] However, during infection, the stiff competition for space and nutrients results in a significant decline in the bacterial density of such genera.[45] The production of bacteriocins directly kills these genera.[47] In a nutshell, the metabolic needs of these genera significantly differ from those of *M.tb* in that they cannot co-exist in the same environment. They, hence, are enriched in the uninfected airways. Currently, we don't know if these bacterial genera exert any immunomodulatory or stimulatory effect.

Using a microbiome-centric analysis, we identified a novel signature that accurately discriminated active TB from LTBI and the *M.tb*-uninfected. Simultaneous appearance of *M.tb* infection with other bacterial infections is not common. Such occurrence has been reported in both immunodeficient[48] and immunocompetent states.[49] *Neisseria species* are generally considered non-pathogenic. In the setting of *M.tb* infection, *Neisseria mucosa* has been reported to cause atypical infection.[50] Several studies have reported *Fusobacterium* and *Prevotella* as common genera in the airways of individuals with active TB.[15,21,51–53] *Actinomyces* including *Schaalia* have also been described in *M.tb*-infection.[54–57] In other scenarios, these bacteria cause infections that mimic *M.tb* infection.[58,59] It is also worth mentioning that *actinomycetes* are notorious producers of antibiotics.[60,61] *Brevibacillus* is known for its production of a lipopeptide, brevibacillin, with potent antimycobacterial activity.[62,63] Other metabolites produced by *Brevibacillus* such as Laterosporulin10 are also critical in antimicrobial defense.[64,65] *Microbacterium* is an environmental bacteria. In most cases, it is considered a contaminant upon isolation. In the context of *M.tb* infection, little is known about this bacteria. However, it is very critical in the biodegradation of sulfonamide antibiotics and heavy metals.[66,67]

To date, the utility of a microbiome signature as a TB diagnostic has not been realized yet in the TB world of diagnostics. Although our findings provide a preliminary picture of an airway microbiome-based TB signature, several questions need to be answered. Defining microbiome signature combinations with higher predictive power is a work in progress. It requires careful iterations of individual signatures, tested using multiple predictive models in large cohorts of well-characterized TB-infected individuals. Furthermore, the sensitivity and specificity of microbiome signatures must be carefully assessed, considering several factors such as prior antibiotic use, different geographic settings, and potential confounders such as age, sex, body mass index, nutrition, HIV status, respiratory comorbidities, and smoking status. However, with robust biostatistical tools that control for microbiome confounders in microbiome-wide association studies such as MetadeconfoundR,[68,69] and LongDat,[70] such hurdles can easily be overcome. In our study, a careful interrogation of potential confounders such as COPD, HIV, and antibiotic use was carefully considered. An additional look at the metabolites produced by these signatures could be valuable. Teasing out the direct influence of IFNγ levels on microbiome diversity is a critical step that needs to be taken to decipher signatures predicting TB outcomes. Validation of the microbiome signatures in large ongoing multicenter TB trials will be critical to addressing gaps in refining microbiome signatures as biomarkers of TB susceptibility and disease progression.

Limitations of the study

In this study, we analyzed the microbiome to the genus level using 16S amplicon sequence data. A deeper interrogation of the above signatures at a species level would be critical in illuminating further their utility as predictors of TB outcomes. Furthermore, as previously noted, we did not tease out the direct influence of IFNγ levels on microbiome diversity, a critical step that needs to be undertaken to decipher signatures predicting TB outcomes.

STAR★METHODS

Detailed methods are provided in the online version of this paper and include the following:

- KEY RESOURCES TABLE
- RESOURCE AVAILABILITY
  - Lead contact
  - Materials availability

- Data and code availability
- EXPERIMENTAL MODEL AND STUDY PARTICIPANT DETAILS
  - Participant screening and enrollment
  - Ethical considerations
- METHOD DETAILS
  - Sputum induction and blood sample collection
  - Blood collection and processing for QFT assays
  - IFNγ ELISA
  - Sputum processing for GeneXpert assay
  - 16S rRNA amplicon sequencing
  - Quality control for 16S amplicon sequencing
- QUANTIFICATION AND STATISTICAL ANALYSIS
  - Exposure and outcome variables
  - Sample size calculation
  - Analysis plan

SUPPLEMENTAL INFORMATION

Supplemental information can be found online at https://doi.org/10.1016/j.isci.2024.110142.

ACKNOWLEDGMENTS

We would like to thank the LMB and HLM research teams, ACCESS Uganda, and Nakaseke General Hospital for the administrative support provided. This original research article was funded by grants supported by the US National Institutes of Health through the Fogarty International Center, NIH Award numbers: R21TW012354, titled Investigating the role of altered lung microbiome in driving Th17-mediated airway inflammation in HIV-associated COPD in rural Uganda and D43TW009093, titled Training of Ugandans in Basic and Translational Research on TB and Emerging Infectious Diseases. Its contents are solely the authors' responsibility and do not necessarily represent the official views of the supporting offices.

AUTHOR CONTRIBUTIONS

Conceptualization, A.K., O.J.S., and H.M.K.; Analysis, A.K., G.O., and M.L.N.; Data curation, A.K., G.O., and M.L.N.; investigation, R.M., M.L.N., W.S., J.N., G.O., and M.L.N.; writing-original draft, A.K.; Writing-review and editing, H.M.K., D.J., O.J.S., K.S., E.K., R.K., D.P.K., and B.S.B.; Visualization, A.K., G.O., and M.L.N.; Supervision, O.J.S., M.L.J., and H.M.K.

DECLARATION OF INTERESTS

All Authors declared no conflicts of interest.

Received: January 29, 2024
Revised: March 5, 2024
Accepted: May 27, 2024
Published: May 28, 2024

REFERENCES

1. Bagcchi, S. (2023). WHO's global tuberculosis report 2022. Lancet Microbe *4*, E20. https://doi.org/10.1016/S2666-5247(22)00359-7.
2. Wang, Z., Arat, S., Magid-Slav, M., and Brown, J.R. (2018). Meta-analysis of human gene expression in response to Mycobacterium tuberculosis infection reveals potential therapeutic targets. BMC Syst. Biol. *12*, 3–18. https://doi.org/10.1186/s12918-017-0524-z.
3. Palucci, I., and Delogu, G. (2018). Host directed therapies for tuberculosis: futures strategies for an ancient disease. Chemotherapy *63*, p172–p180. https://doi.org/10.1159/000490478.
4. Marakalala, M.J., Martinez, F.O., Plüddemann, A., and Gordon, S. (2018). Macrophage heterogeneity in the immunopathogenesis of tuberculosis. Front. Microbiol. *9*, 366433. https://doi.org/10.3389/fmicb.2018.01028.
5. Arnold, I.C., Hutchings, C., Kondova, I., Hey, A., Powrie, F., Beverley, P., and Tchilian, E. (2015). Helicobacter hepaticus infection in BALB/c mice abolishes subunit-vaccine-induced protection against M. tuberculosis. Vaccine *33*, 1808–1814. https://doi.org/10.1016/j.vaccine.2015.02.041.
6. Majlessi, L., Sayes, F., Bureau, J.F., Pawlik, A., Michel, V., Jouvion, G., Huerre, M., Severgnini, M., Consolandi, C., Peano, C., et al. (2017). Colonization with Helicobacter is concomitant with modified gut microbiota and drastic failure of the immune control of Mycobacterium tuberculosis. Mucosal Immunol. *10*, 1178–1189. https://doi.org/10.1038/mi.2016.140.
7. Negatu, D.A., Liu, J.J.J., Zimmerman, M., Kaya, F., Dartois, V., Aldrich, C.C., Gengenbacher, M., and Dick, T. (2018). Whole-cell screen of fragment library identifies gut microbiota metabolite indole propionic acid as antitubercular. Antimicrob. Agents Chemother. *62*, e01571-17. https://doi.org/10.1128/aac.01571-17.
8. Kaufmann, S.H.E. (2018). Indole propionic acid: a small molecule links between gut microbiota and tuberculosis. Antimicrob. Agents Chemother. *62*, e00389-18. https://doi.org/10.1128/aac.00389-18.
9. Khan, N., Vidyarthi, A., Nadeem, S., Negi, S., Nair, G., and Agrewala, J.N. (2016). Alteration in the gut microbiota provokes susceptibility to tuberculosis. Front. Immunol. *7*, 529. https://doi.org/10.3389/fimmu.2016.00529.

10. Luo, M., Liu, Y., Wu, P., Luo, D.X., Sun, Q., Zheng, H., Hu, R., Pandol, S.J., Li, Q.F., Han, Y.P., et al. (2017). Alternation of gut microbiota in patients with pulmonary tuberculosis. Front. Physiol. *8*, 822. https://doi.org/10.3389/fphys.2017.00822.
11. Maji, A., Misra, R., Dhakan, D.B., Gupta, V., Mahato, N.K., Saxena, R., Mittal, P., Thukral, N., Sharma, E., Singh, A., et al. (2018). Gut microbiome contributes to impairment of immunity in pulmonary tuberculosis patients by alteration of butyrate and propionate producers. Environ. Microbiol. *20*, 402–419. https://doi.org/10.1111/1462-2920.14015.
12. Corrêa-Oliveira, R., Fachi, J.L., Vieira, A., Sato, F.T., and Vinolo, M.A.R. (2016). Regulation of immune cell function by short-chain fatty acids. Clin. Transl. Immunol. *5*, e73. https://doi.org/10.1038/cti.2016.17.
13. Lachmandas, E., van den Heuvel, C.N.A.M., Damen, M.S.M.A., Cleophas, M.C.P., Netea, M.G., and van Crevel, R. (2016). Diabetes mellitus and increased tuberculosis susceptibility: the role of short-chain fatty acids. J. Diabetes Res. *2016*, 6014631. https://doi.org/10.1155/2016/6014631.
14. Krishna, P., Jain, A., and Bisen, P.S. (2016). Microbiome diversity in the sputum of patients with pulmonary tuberculosis. Eur. J. Clin. Microbiol. Infect. Dis. *35*, 1205–1210. https://doi.org/10.1007/s10096-016-2654-4.
15. Wu, J., Liu, W., He, L., Huang, F., Chen, J., Cui, P., Shen, Y., Zhao, J., Wang, W., Zhang, Y., et al. (2013). Sputum microbiota associated with new, recurrent and treatment failure tuberculosis. PLoS One *8*, e83445. https://doi.org/10.1371/journal.pone.0083445.
16. Hong, B.Y., Paulson, J.N., Stine, O.C., Weinstock, G.M., and Cervantes, J.L. (2018). Meta-analysis of the lung microbiota in pulmonary tuberculosis. Tuberculosis *109*, 102–108. https://doi.org/10.1016/j.tube.2018.02.006.
17. Zhou, Y., Lin, F., Cui, Z., Zhang, X., Hu, C., Shen, T., Chen, C., Zhang, X., and Guo, X. (2015). Correlation between either Cupriavidus or Porphyromonas and primary pulmonary tuberculosis found by analysing the microbiota in patients' bronchoalveolar lavage fluid. PLoS One *10*, e0124194. https://doi.org/10.1371/journal.pone.0124194.
18. Segal, L.N., Clemente, J.C., Li, Y., Ruan, C., Cao, J., Danckers, M., Morris, A., Tapyrik, S., Wu, B.G., Diaz, P., et al. (2017). Anaerobic bacterial fermentation products increase tuberculosis risk in antiretroviral-drug-treated HIV patients. Cell Host Microbe *21*, 530–537.e4. https://doi.org/10.1016/j.chom.2017.03.003.
19. Wipperman, M.F., Fitzgerald, D.W., Juste, M.A.J., Taur, Y., Namasivayam, S., Sher, A., Bean, J.M., Bucci, V., and Glickman, M.S. (2017). Antibiotic treatment for Tuberculosis induces a profound dysbiosis of the microbiome that persists long after therapy is completed. Sci. Rep. *7*, 10767. https://doi.org/10.1038/s41598-017-10346-6.
20. Mori, G., Morrison, M., and Blumenthal, A. (2021). Microbiome-immune interactions in tuberculosis. PLoS Pathog. *17*, e1009377. https://doi.org/10.1371/journal.ppat.1009377.
21. Naidoo, C.C., Nyawo, G.R., Wu, B.G., Walzl, G., Warren, R.M., Segal, L.N., and Theron, G. (2019). The microbiome and tuberculosis: state of the art, potential applications, and defining the clinical research agenda. Lancet Respir. Med. *7*, 892–906. https://doi.org/10.1016/S2213-2600(18)30501-0.
22. Musisi, E., Wyness, A., Eldirdiri, S., Dombay, E., Mtafya, B., Ntinginya, N.E., Heinrich, N., Kibiki, G.S., Hoelscher, M., Boeree, M., et al. (2023). Effect of seven anti-tuberculosis treatment regimens on sputum microbiome: a retrospective analysis of the HIGHRIF study 2 and PanACEA MAMS-TB clinical trials. Lancet Microbe *4*, e913–e922. https://doi.org/10.1016/S2666-5247(23)00191-X.
23. Somboro, A.M., Diallo, D., Holl, J.L., and Maiga, M. (2021). The role of the microbiome in inflammation during tuberculosis. EBioMedicine *68*, 103435. https://doi.org/10.1016/j.ebiom.2021.103435.
24. Baral, T., Kurian, S.J., Sekhar, S., Munisamy, M., Kudru, C.U., Khandelwal, B., Banerjee, M., Mukhopadhyay, C., Saravu, K., Singh, J., and Singh, S. (2022). Role of the gut microbiome and probiotics for prevention and management of tuberculosis. In Microbiome, Immunity, Digestive Health and Nutrition (Elsevier), pp. 361–371. https://doi.org/10.1016/B978-0-12-822238-6.00036-4.
25. Siddharthan, T., Grigsby, M., Morgan, B., Kalyesubula, R., Wise, R.A., Kirenga, B., and Checkley, W. (2019). Prevalence of chronic respiratory disease in urban and rural Uganda. Bull. World Health Organ. *97*, 318–327. https://doi.org/10.2471/BLT.18.216523.
26. Kayongo, A., Wosu, A.C., Naz, T., Nassali, F., Kalyesubula, R., Kirenga, B., Wise, R.A., Siddharthan, T., and Checkley, W. (2020). Chronic obstructive pulmonary disease prevalence and associated factors in a setting of well-controlled HIV, a cross-sectional study. COPD *17*, 297–305. https://doi.org/10.1080/15412555.2020.1769583.
27. Verrall, A.J., Alisjahbana, B., Apriani, L., Novianty, N., Nurani, A.C., van Laarhoven, A., Ussher, J.E., Indrati, A., Ruslami, R., Netea, M.G., et al. (2020). Early clearance of Mycobacterium tuberculosis: the INFECT case contact cohort study in Indonesia. J. Infect. Dis. *221*, 1351–1360. https://doi.org/10.1093/infdis/jiz168.
28. Mave, V., Chandrasekaran, P., Chavan, A., Shivakumar, S.V.B.Y., Danasekaran, K., Paradkar, M., Thiruvengadam, K., Kinikar, A., Murali, L., Gaikwad, S., et al. (2019). Infection free "resisters" among household contacts of adult pulmonary tuberculosis. PLoS One *14*, e0218034. https://doi.org/10.1371/journal.pone.0218034.
29. Kroon, E.E., Kinnear, C.J., Orlova, M., Fischinger, S., Shin, S., Boolay, S., Walzl, G., Jacobs, A., Wilkinson, R.J., Alter, G., et al. (2020). An observational study identifying highly tuberculosis-exposed, HIV-1-positive but persistently TB, tuberculin and IGRA negative persons with M. tuberculosis specific antibodies in Cape Town, South Africa. EBioMedicine *61*, 103053. https://doi.org/10.1016/j.ebiom.2020.103053.
30. Seedat, F., James, I., Loubser, S., Waja, Z., Mallal, S.A., Hoffmann, C., Tiemessen, C.T., Chaisson, R.E., and Martinson, N.A. (2021). Human leukocyte antigen associations with protection against tuberculosis infection and disease in human immunodeficiency virus-1 infected individuals, despite household tuberculosis exposure and immune suppression. Tuberculosis *126*, 102023. https://doi.org/10.1016/j.tube.2020.102023.
31. Ma, N., Zalwango, S., Malone, L.L., Nsereko, M., Wampande, E.M., Thiel, B.A., Okware, B., Igo, R.P., Joloba, M.L., Mupere, E., et al. (2014). Clinical and epidemiological characteristics of individuals resistant to M. tuberculosis infection in a longitudinal TB household contact study in Kampala, Uganda. BMC Infect. Dis. *14*, 352. https://doi.org/10.1186/1471-2334-14-352.
32. McHenry, M.L., Benchek, P., Malone, L.S., Nsereko, M., Mayanja-Kizza, H., Boom, W.H., Williams, S.M., Hawn, T.R., and Stein, C.M. (2021). Resistance to TST/IGRA conversion in Uganda: heritability and Genome-Wide association study. EBioMedicine *74*, 103727. https://doi.org/10.1016/j.ebiom.2021.103727.
33. Stein, C.M., Nsereko, M., Malone, L.L., Okware, B., Kisingo, H., Nalukwago, S., Chervenak, K., Mayanja-Kizza, H., Hawn, T.R., and Boom, W.H. (2019). Long-term stability of resistance to latent Mycobacterium tuberculosis infection in highly exposed tuberculosis household contacts in Kampala, Uganda. Clin. Infect. Dis. *68*, 1705–1712. https://doi.org/10.1093/cid/ciy751.
34. Lu, L.L., Smith, M.T., Yu, K.K.Q., Luedemann, C., Suscovich, T.J., Grace, P.S., Cain, A., Yu, W.H., McKitrick, T.R., Lauffenburger, D., et al. (2019). IFN-γ-independent immune markers of Mycobacterium tuberculosis exposure. Nat. Med. *25*, 977–987. https://doi.org/10.1038/s41591-019-0441-3.
35. Stein, C.M. (2023). Genetic epidemiology of resistance to M. tuberculosis Infection: importance of study design and recent findings. Gene Immun. *24*, 117–123. https://doi.org/10.1038/s41435-023-00204-z.
36. Davies, L.R.L., Smith, M.T., Cizmeci, D., Fischinger, S., Shih-Lu Lee, J., Lu, L.L., Layton, E.D., Grant, A.D., Fielding, K., Stein, C.M., et al. (2023). IFN-γ independent markers of Mycobacterium tuberculosis exposure among male South African gold miners. EBioMedicine *93*, 104678. https://doi.org/10.1016/j.ebiom.2023.104678.
37. Guwatudde, D., Zalwango, S., Kamya, M.R., Debanne, S.M., Diaz, M.I., Okwera, A., Mugerwa, R.D., King, C., and Whalen, C.C. (2003). Burden of tuberculosis in Kampala, Uganda. Bull. World Health Organ. *81*, 799–805.
38. Smith, J.P., Oeltmann, J.E., Hill, A.N., Tobias, J.L., Boyd, R., Click, E.S., Finlay, A., Mondongo, C., Zetola, N.M., and Moonan, P.K. (2022). Characterizing tuberculosis transmission dynamics in high-burden urban and rural settings. Sci. Rep. *12*, 6780. https://doi.org/10.1038/s41598-022-10488-2.
39. Chamie, G., Kato-Maeda, M., Emperador, D.M., Wandera, B., Mugagga, O., Crandall, J., Janes, M., Marquez, C., Kamya, M.R., Charlebois, E.D., and Havlir, D.V. (2018). Spatial overlap links seemingly unconnected genotype-matched TB cases in rural Uganda. PLoS One *13*, e0192666. https://doi.org/10.1371/journal.pone.0192666.
40. Mayito, J., Martineau, A.R., Tiwari, D., Nakiyingi, L., Kateete, D.P., Reece, S.T., and Biraro, I.A. (2023). Determinants of QuantiFERON Plus-diagnosed tuberculosis infection in adult Ugandan TB contacts: A cross-sectional study. PLoS One *18*, e0281559. https://doi.org/10.1371/journal.pone.0281559.
41. Kern, L., Abdeen, S.K., Kolodziejczyk, A.A., and Elinav, E. (2021). Commensal inter-bacterial interactions shaping the microbiota. Curr. Opin. Microbiol. *63*, 158–171. https://doi.org/10.1016/j.mib.2021.07.011.
42. Liu, C.H., Liu, H., and Ge, B. (2017). Innate immunity in tuberculosis: host defense vs pathogen evasion. Cell. Mol. Immunol. *14*,

963–975. https://doi.org/10.1038/cmi.2017.88.
43. Mayer-Barber, K.D., Andrade, B.B., Barber, D.L., Hieny, S., Feng, C.G., Caspar, P., Oland, S., Gordon, S., and Sher, A. (2011). Innate and adaptive interferons suppress IL-1α and IL-1β production by distinct pulmonary myeloid subsets during Mycobacterium tuberculosis infection. Immunity *35*, 1023–1034. https://doi.org/10.1016/j.immuni.2011.12.002.
44. Cadena, A.M., Fortune, S.M., and Flynn, J.L. (2017). Heterogeneity in tuberculosis. Nat. Rev. Immunol. *17*, 691–702. https://doi.org/10.1038/nri.2017.69.
45. Pérez-Cobas, A.E., Rodríguez-Beltrán, J., Baquero, F., and Coque, T.M. (2023). Ecology of the respiratory tract microbiome. Trends Microbiol. *31*, 972–984. https://doi.org/10.1016/j.tim.2023.04.006.
46. Nagashima, K., Zhao, A., Atabakhsh, K., Bae, M., Blum, J.E., Weakley, A., Jain, S., Meng, X., Cheng, A.G., Wang, M., et al. (2023). Mapping the T cell repertoire to a complex gut bacterial community. Nature *621*, 162–170. https://doi.org/10.1038/s41586-023-06431-8.
47. Zheng, J., Gänzle, M.G., Lin, X.B., Ruan, L., and Sun, M. (2015). Diversity and dynamics of bacteriocins from human microbiome. Environ. Microbiol. *17*, 2133–2143. https://doi.org/10.1111/1462-2920.12662.
48. Rabuñal, R., Corredoira, J., Monte, R., and Coira, A. (2009). Co-infection by Streptococcus anginosus and Mycobacterium tuberculosis: three case reports. J. Med. Case Rep. *3*, 1–3. https://doi.org/10.1186/1752-1947-3-37.
49. Saldaña, N.G., Bejarano, J.I.C., Porras, M.H., de la Garza, E.A., Gutiérrez, S.F., Gutiérrez, J.L.C., and Olguin, H.J. (2020). Co-infection with Streptococcus anginosus and Mycobacterium tuberculosis in an immunocompetent pediatric patient. A case report. BMC Pulm. Med. *20*, 1–5. https://doi.org/10.1186/s12890-019-1044-y.
50. Hioki, T., Soejima, K., Goto, Y., Sugiura, M., Umemura, T., Ishihara, Y., Mutoh, Y., Sakanashi, D., and Mikamo, H. (2024). Co-infection with Neisseria mucosa in a patient with tuberculous otitis media. J. Otolaryngol. *19*, 1–4. https://doi.org/10.1016/j.joto.2023.10.001.
51. Cheung, M.K., Lam, W.Y., Fung, W.Y.W., Law, P.T.W., Au, C.H., Nong, W., Kam, K.M., Kwan, H.S., and Tsui, S.K.W. (2013). Sputum microbiota in tuberculosis as revealed by 16S rRNA pyrosequencing. PLoS One *8*, e54574. https://doi.org/10.1371/journal.pone.0054574.
52. Ticlla, M.R., Hella, J., Hiza, H., Sasamalo, M., Mhimbira, F., Rutaihwa, L.K., Droz, S., Schaller, S., Reither, K., Hilty, M., et al. (2021). The sputum microbiome in pulmonary tuberculosis and its association with disease manifestations: a cross-sectional study. Front. Microbiol. *12*, 633396. https://doi.org/10.3389/fmicb.2021.633396.
53. Perveen, S., and Sharma, R. (2022). Lung Microbiome: Friend or Foe of Mycobacterium tuberculosis. In Microbiome in Inflammatory Lung Diseases, G. Gupta, B.G. Oliver, K. Dua, A. Singh, and R. MacLoughlin, eds. (Springer), pp. 207–226. Book chapter. https://doi.org/10.1007/978-981-16-8957-4_12.
54. Tietz, A., Aldridge, K.E., and Figueroa, J.E. (2005). Disseminated coinfection with Actinomyces graevenitzii and Mycobacterium tuberculosis: case report and review of the literature. J. Clin. Microbiol. *43*, 3017–3022. https://doi.org/10.1128/jcm.43.6.3017-3022.2005.
55. Chen, Y., and Hu, W. (2023). Co-infection with Mycobacterium tuberculosis and Nocardia farcinica in a COPD patient: a case report. BMC Pulm. Med. *23*, 136. https://doi.org/10.1186/s12890-023-02434-3.
56. Könönen, E., and Wade, W.G. (2015). Actinomyces and related organisms in human infections. Clin. Microbiol. Rev. *28*, 419–442. https://doi.org/10.1128/cmr.00100-14.
57. El Hammoumi, M.M., Bhairis, M., Essotina, A.A., and Kabiri, E.H. (2018). Association of pulmonary actinomycosis and tuberculosis: a very rare finding. J. Case Rep. Med. *7*, 1–3. https://doi.org/10.15761/JCRM.1000107.
58. Gliga, S., Devaux, M., Gosset Woimant, M., Mompoint, D., Perronne, C., and Davido, B. (2014). Actinomyces graevenitzii pulmonary abscess mimicking tuberculosis in a healthy young man. Can. Respir. J. J. Can. Thorac. Soc. *21*, e75–e77. https://doi.org/10.1155/2014/841480.
59. Franco-Paredes, C. (2014). Aerobic actinomycetes that masquerade as pulmonary tuberculosis. Bol. Médico Hosp. Infant. México *71*, 37–40.
60. Takahashi, Y., and Nakashima, T. (2018). Actinomycetes, an inexhaustible source of naturally occurring antibiotics. Antibiotics *7*, 45.
61. De Simeis, D., and Serra, S. (2021). Actinomycetes: A never-ending source of bioactive compounds—An overview on antibiotics production. Antibiotics *10*, 483. https://doi.org/10.3390/antibiotics10050483.
62. Hassi, M., Guendouzi, S.E., Haggoud, A., David, S., Ibnsouda, S., Houari, A., and Iraqui, M. (2012). Antimycobacterial activity of a Brevibacillus laterosporus strain isolated from a Moroccan soil. Braz. J. Microbiol. *43*, 1516–1522. https://doi.org/10.1590/S1517-83822012000400036.
63. Yang, X., Huang, E., Yuan, C., Zhang, L., and Yousef, A.E. (2016). Isolation and structural elucidation of brevibacillin, an antimicrobial lipopeptide from Brevibacillus laterosporus that combats drug-resistant Gram-positive bacteria. Appl. Environ. Microbiol. *82*, 2763–2772. https://doi.org/10.1128/AEM.00315-16.
64. Baindara, P., Singh, N., Ranjan, M., Nallabelli, N., Chaudhry, V., Pathania, G.L., Sharma, N., Kumar, A., Patil, P.B., and Korpole, S. (2016). Laterosporulin10: a novel defensin like class IId bacteriocin from Brevibacillus sp. strain SKDU10 with inhibitory activity against microbial pathogens. Microbiology *162*, 1286–1299. https://doi.org/10.1099/mic.0.000316.
65. Yang, X., and Yousef, A.E. (2018). Antimicrobial peptides produced by Brevibacillus spp.: structure, classification and bioactivity: a mini review. World J. Microbiol. Biotechnol. *34*, 57. https://doi.org/10.1007/s11274-018-2437-4.
66. Topp, E., Chapman, R., Devers-Lamrani, M., Hartmann, A., Marti, R., Martin-Laurent, F., Sabourin, L., Scott, A., and Sumarah, M. (2013). Accelerated Biodegradation of Veterinary Antibiotics in Agricultural Soil following Long-Term Exposure, and Isolation of a Sulfamethazine-degrading sp. J. Environ. Qual. *42*, 173–178. https://doi.org/10.2134/jeq2012.0162.
67. Ricken, B., Fellmann, O., Kohler, H.P.E., Schäffer, A., Corvini, P.F.X., and Kolvenbach, B.A. (2015). Degradation of sulfonamide antibiotics by Microbacterium sp. strain BR1–elucidating the downstream pathway. N. Biotech. *32*, 710–715. https://doi.org/10.1016/j.nbt.2015.03.005.
68. Fromentin, S., Forslund, S.K., Chechi, K., Aron-Wisnewsky, J., Chakaroun, R., Nielsen, T., Tremaroli, V., Ji, B., Prifti, E., Myridakis, A., et al. (2022). Microbiome and metabolome features of the cardiometabolic disease spectrum. Nat. Med. *28*, 303–314. https://doi.org/10.1038/s41591-022-01688-4.
69. Fan, Y., Støving, R.K., Berreira Ibraim, S., Hyötyläinen, T., Thirion, F., Arora, T., Lyu, L., Stankevic, E., Hansen, T.H., Déchelotte, P., et al. (2023). The gut microbiota contributes to the pathogenesis of anorexia nervosa in humans and mice. Nat. Microbiol. *8*, 787–802. https://doi.org/10.1038/s41564-023-01355-5.
70. Chen, C.-Y., Löber, U., and Forslund, S.K. (2023). LongDat: an R package for covariate-sensitive longitudinal analysis of high-dimensional data. Bioinform. Adv. *3*, vbad063. https://doi.org/10.1093/bioadv/vbad063.
71. Mende, D.R., Letunic, I., Maistrenko, O.M., Schmidt, T.S.B., Milanese, A., Paoli, L., Hernández-Plaza, A., Orakov, A.N., Forslund, S.K., Sunagawa, S., et al. (2020). proGenomes2: an improved database for accurate and consistent habitat, taxonomic and functional annotations of prokaryotic genomes. Nucleic Acids Res. *48*, D621–D625. https://doi.org/10.1093/nar/gkz1002.
72. Hildebrand, F., Tadeo, R., Voigt, A.Y., Bork, P., and Raes, J. (2014). LotuS: an efficient and user-friendly OTU processing pipeline. Microbiome *2*, 30–37. https://doi.org/10.1186/2049-2618-2-30.
73. Edgar, R.C. (2013). UPARSE: highly accurate OTU sequences from microbial amplicon reads. Nat. Methods *10*, 996–998. https://doi.org/10.1038/nmeth.2604.
74. Quast, C., Pruesse, E., Yilmaz, P., Gerken, J., Schweer, T., Yarza, P., Peplies, J., and Glöckner, F.O. (2013). The SILVA ribosomal RNA gene database project: improved data processing and web-based tools. Nucleic Acids Res. *41*, D590–D596. https://doi.org/10.1093/nar/gks1219.
75. Saary, P., Forslund, K., Bork, P., and Hildebrand, F. (2017). RTK: efficient rarefaction analysis of large datasets. Bioinformatics *33*, 2594–2595. https://doi.org/10.1093/bioinformatics/btx206.
76. Thandapani, P., Kloetgen, A., Witkowski, M.T., Glytsou, C., Lee, A.K., Wang, E., Wang, J., LeBoeuf, S.E., Avrampou, K., Papagiannakopoulos, T., et al. (2022). Valine tRNA levels and availability regulate complex I assembly in leukaemia. Nature *601*, 428–433. https://doi.org/10.1038/s41586-021-04244-1.
77. Ho, X.D., Phung, P., Q Le, V., H Nguyen, V., Reimann, E., Prans, E., Kõks, G., Maasalu, K., Le, N.T., H Trinh, L., et al. (2017). Whole transcriptome analysis identifies differentially regulated networks between osteosarcoma and normal bone samples. Exp. Biol. Med. *242*, 1802–1811. https://doi.org/10.1177/1535370217736512.
78. Forslund, S.K., Chakaroun, R., Zimmermann-Kogadeeva, M., Markó, L., Aron-Wisnewsky, J., Nielsen, T., Moitinho-Silva, L., Schmidt, T.S.B., Falony, G., Vieira-Silva, S., et al. (2021). Combinatorial, additive and dose-dependent drug–microbiome associations. Nature *600*, 500–505. https://doi.org/10.1038/s41586-021-04177-9.
79. Kayongo, A., Bartolomaeus, T.U.P., Birkner, T., Markó, L., Löber, U., Kigozi, E., Atugonza,

C., Munana, R., Mawanda, D., Sekibira, R., et al. (2023). Sputum microbiome and chronic obstructive pulmonary disease in a rural Ugandan cohort of well-controlled HIV infection. Microbiol. Spectr. *11*, e0213921. https://doi.org/10.1128/spectrum.02139-21.

80. Loens, K., Van Heirstraeten, L., Malhotra-Kumar, S., Goossens, H., and Ieven, M. (2009). Optimal sampling sites and methods for detection of pathogens possibly causing community-acquired lower respiratory tract infections. J. Clin. Microbiol. *47*, 21–31. https://doi.org/10.1128/jcm.02037-08.

81. Gershman, N.H., Liu, H., Wong, H.H., Liu, J.T., and Fahy, J.V. (1999). Fractional analysis of sequential induced sputum samples during sputum induction: evidence that different lung compartments are sampled at different time points. J. Allergy Clin. Immunol. *104*, 322–328. https://doi.org/10.1016/S0091-6749(99)70374-X.

82. Holmes, I., Harris, K., and Quince, C. (2012). Dirichlet multinomial mixtures: generative models for microbial metagenomics. PLoS One *7*, e30126. https://doi.org/10.1371/journal.pone.0030126.

STAR★METHODS

KEY RESOURCES TABLE

REAGENT or RESOURCE	SOURCE	IDENTIFIER
Chemicals, peptides, and recombinant proteins		
341F (5′ NNNNNNNNNNCCT ACGGGNGGCWGCAG)	LGC Biosearch Tech	341F
785R (5′ NNNNNNNNNNGACTA CHVGGGTATCTAAKCC)	LGC Biosearch Tech	785R
MyTaq buffer	Bioline GmbH	MyTaq buffer
MyTaq DNA polymerase	Bioline GmbH	MyTaq DNA poly
BioStabII PCR Enhancer	Sigma-Aldrich Co	BioStabII
Critical commercial assays		
Xpert MTB/RIF Cepheid kit	Cepheid	GXMTB/RIF-US-10
QuantiFERON-Gold (QFT) tubes	Qiagen	Catalog. no. 622130
IFNγ ELISA kits	Qiagen	Catalog. no. 622130
DNA collection, preservation, and isolation kit	Norgen Biotek Corp	Catalog no.RU46100
Deposited data		
Metadata	Mendeley Data https://data.mendeley.com/preview/vwt6g5gp22	https://doi.org/10.17632/vwt6g5gp22.1
Raw 16S reads	Mendeley Data https://data.mendeley.com/drafts/gf3vxvptsd	https://doi.org/10.17632/gf3vxvptsd.1.
Processed Sequences	Mendeley Data https://data.mendeley.com/preview/vwt6g5gp22	https://doi.org/10.17632/vwt6g5gp22.1
Code	Mendeley Data https://data.mendeley.com/preview/vwt6g5gp22	https://doi.org/10.17632/vwt6g5gp22.1
Software and algorithms		
ProGenomes2 microbial genome database	Mende et al., 2020[71]	Hildebrand et al., 2014[72]
LotuS, version 1.62.	Hildebrand et al., 2014[72]	Mende et al., 2020[71]
UPARSE	Edgar et al., 2013[73]	Edgar et al., 2013[73]
SILVA	Quast et al., 2012[74]	Quast et al., 2012[74]
RTK version 0.93.1	Saary et al., 2017[75]	Saary et al., 2017[75]
EdgeR, version 3.14.0	Thandapani et al., 2022[76]	Thandapani et al., 2022[76]
DESeq2, version 1.43.1	Ho, Xuan Dunge t al., 2017[77]	Ho et al.,[77]
MetadeconfoundR	Forslund et al., 2021[78]	Forslund et al.,[78]

RESOURCE AVAILABILITY

Lead contact

Further information and requests for resources and reagents should be directed to and will be fulfilled by the lead contact, Dr Alex Kayongo at email address: akayongo@chs.mak.ac.ug.

Materials availability

This study did not generate new unique reagents.

Data and code availability

- De-identified human data is deposited at Mendeley Data, V1, https://doi.org/10.17632/vwt6g5gp22.1. as metadata. Raw and processed 16S sequences are deposited at Mendeley Data, V1, https://doi.org/10.17632/gf3vxvptsd.1. and Mendeley Data, V1,

https://doi.org/10.17632/vwt6g5gp22.1. respectively, and is publicly available as of the date of publication. DOIs are listed in the key resources table.

- All original code has been deposited at Mendeley Data, V1, https://doi.org/10.17632/vwt6g5gp22.1, and is publicly available as of the date of publication. DOIs are listed in the key resources table.
- Any additional information required to reanalyze the data reported in this paper is available from the lead contact upon request.

EXPERIMENTAL MODEL AND STUDY PARTICIPANT DETAILS

Participant screening and enrollment

We screened for *M.tb* infection using QuantiFERON-TB Gold and GeneXpert assays on participants previously enrolled in an existing HIV Lung Microbiome cohort established in rural Uganda.[79] Briefly, the HLM cohort is a longitudinal cohort established in 2018 comprised of 200 individuals stratified by HIV and COPD status.[79] From February 2018 to February 2021, the HLM cohort was randomly recruited from two large independent cohorts, i.e., The Lung Function study in Kampala and Nakaseke (LiNK, comprised of n=656 HIV-negative individuals) and the HIV-infected Lung Function study in Nakaseke (HiLiNK, comprised of n=722 HIV-positive individuals)[26] in the same geographic location. The HLM cohort was comprised of 50 HIV+COPD+ individuals, 50 HIV+COPD- individuals, 50 HIV-COPD+ individuals, and 50 HIV-COPD- individuals (total n = 200). Participants were eligible for inclusion if they resided within the Nakaseke district, were ≥35 years of age, had confirmed HIV serostatus and spirometry-based COPD status at enrollment, were capable of understanding study procedures, underwent successful sputum induction, had no history of prior antibiotic use in the past two weeks and did not have contraindications for spirometry and sputum induction procedure. During the genesis of the HLM cohort, matching was attempted based on three participant characteristics (age, sex, and smoking status). However, it was limited by a small sampling frame of 50 individuals in the COPD+/HIV− group from the LiNK cohort and COPD+/HIV+ group from the HiLiNK cohort, as well as differences in sociodemographic and clinical characteristics between the LiNK and HiLiNK cohort. To control for these matching limitations, the study team determined the differences in the distribution of sociodemographic characteristics across the main groups (COPD+/HIV+, COPD−/HIV+, COPD+/HIV−, COPD−/HIV−) and used post-hoc testing for the role of these covariates using a confounder-aware statistical tool in all downstream analyses.[78] During the follow-up period from April 2022 to January 2023, we collected 5mls of induced sputum for the TB GeneXpert test, using the Xpert MTB/RIF kit (Cepheid, USA), from 192 participants and 20mls of peripheral blood for the QFT assay using the QuantiFERON-TB GOLD kit (Qiagen Sciences, Inc., Germantown Road, MD, USA) from 99 individuals who agreed to have their blood drawn. Hence, we performed TB GeneXpert on 192 sputum samples and QFTs on 99 matched blood samples from the same individuals. All assays were performed following the manufacturer's instructions.

Ethical considerations

We obtained written informed consent from all study participants. Ethical approval was granted by the Mulago Hospital Research and Ethics Committee (MHREC) (no.1996 and no. 2152), Makerere University School of Biomedical Sciences Research and Ethics Committee (SBS-REC) (no. SBS-2023-312), and the Uganda National Council for Science and Technology (UNCST) (no. HS2375 and HS2035ES) in Kampala, Uganda.

METHOD DETAILS

Sputum induction and blood sample collection

Before the sputum induction procedure, the following three-step cleansing routine using sterile water was followed: rinsing the mouth (gargling and discarding) three times, clearing the back of the throat followed by discarding, and blowing the nose to minimize contamination with saliva or postnasal drip. Each sputum sample was assessed for mucoid consistency upon deep coughing and expectoration, and Gram's stain procedure was performed for quality assessment. Sputum samples with less than 10 squamous epithelial cells per low-power field (×10) microscopy (indicative of a lower airway sample) passed the quality control check.[80] Otherwise, the sample was rejected, and the induction procedure was repeated. Each participant was instructed to inhale and exhale 3% nebulized hypertonic saline through the mouth with the nose clipped.[81] Three 5-minute nebulizing periods were used during the collection, with a rest period of 2 min. We performed the procedure in a negative pressure sputum booth. During each rest, spirometry was performed to determine the percentage fall in FEV_1. Fifteen (15) minutes post-nebulization, 2 to 4 mL of expectorates were collected in sterile sputum containers. For all successful inductions, after a quality check, a sputum sample was collected in a sputum DNA collection, preservation, and isolation kit (Norgen Biotek Corporation, Canada; catalog no. RU46100) as per the manufacturer's instructions for downstream 16S rRNA sequencing or a sterile sputum container for TB GeneXpert assays.

Blood collection and processing for QFT assays

We collected 20 ml of peripheral blood into a single blood collection tube containing lithium heparin as the anticoagulant. Blood was then transported at room temperature within 1 hour before transferring into QFT tubes (catalog. no. 622130, QIAGEN, 19300 Germantown Road, MD 20874, USA) following the manufacturer's instructions. Briefly, we labeled QFT tubes appropriately, making sure each tube (Nil-negative control, TB1, TB2, and Mitogen-positive control) was easily identifiable by its label. We recorded the time and date of blood collection and

ensured that blood collection tubes were kept at room temperature at the time of blood collection. For each participant, we transferred 1ml of collected blood into each of the QFT blood collection tubes following the manufacturer's instructions. Immediately after filling the QFT tubes, we shook them 10 times firmly enough to make sure the entire inner surface of the tube was coated with blood. Following labeling, filling, and shaking, the tubes were transferred to a 37°C incubator within 1 hour of collection and incubated UPRIGHT at 37°C for 24 hours. After incubation of the blood collection tubes at 37°C, we harvested the plasma by centrifuging the QFT tubes for 15 minutes at 2000g using a pipet. Harvested plasma samples were stored at –20°C.

IFNγ ELISA

We used IFNγ ELISA kits from Qiagen (catalog. no. 622130, QIAGEN, 19300 Germantown Road, Germantown, MD 20874, USA) following the manufacturer's instructions. Briefly, plasma samples and reagents, except for conjugate 100x concentrate, were brought to room temperature before use. We allowed at least 1 hour for equilibration. We reconstituted the IFNγ Standard with the volume of distilled water indicated on the label of the vial. We mixed gently to minimize frothing, ensuring that the entire content of the vial was completely dissolved. Reconstitution of the IFNγ standard to the correct volume produced a solution with a concentration of 8.0 IU/ml. Using the reconstituted standard, we prepared a serial dilution of four IFNγ concentrations, and we generated a standard curve with these concentrations. We prepared fresh dilutions of the kit standard for each ELISA session. We reconstituted lyophilized conjugate 100x concentrate with 0.3 ml of distilled water and then mixed gently to minimize frothing, ensuring that the entire content of the vial was completely dissolved. We thoroughly mixed the stored sample before addition to the ELISA well. We added 50 μl of freshly prepared working strength conjugate to each ELISA plate well, followed by 50 μl of test plasma sample to appropriate wells. Finally, we added 50 μl each of the Standards 1-4 to the appropriate plate wells. We covered the ELISA plate and mixed the conjugate and plasma samples/standards thoroughly using a microplate shaker for 1 minute at 500 rpm, avoiding splashing. We covered the ELISA plate and incubated it at room temperature for 2 hours. We took caution not to expose the ELISA plate to direct sunlight. During the ELISA plate incubation, we prepared a working strength wash buffer and diluted one part of Wash Buffer 20x concentrate with 19 parts of distilled water and mixed thoroughly. When ELISA plate incubation was complete, we washed the ELISA plate wells with 400 μl of working strength wash buffer at least 6 times to ensure that each well was filled with wash buffer to the top of the well for each wash cycle. We tapped the ELISA plate face down on an absorbent towel to remove residual wash buffer and added 100 μl of Enzyme Substrate Solution to each plate well, covered the plate, and mixed thoroughly for 1 minute at 500 rpm using a microplate shaker. We covered the ELISA plate and incubated it at room temperature for 30 minutes. Following the 30-minute incubation, we added 50 μl of Enzyme enzyme-stopping solution to each plate well in the same order as the substrate was added and mixed thoroughly at 500 rpm using a microplate shaker. We measured the Optical Density (OD) of ELISA plate wells within 5 minutes of stopping the reaction using a microplate reader fitted with a 450 nm filter and a 650 nm reference filter. OD values were used to calculate the IFNγ concentrations.

Sputum processing for GeneXpert assay

Briefly, upon receipt of the sputum sample in a Biosafety level-3 lab (BSL-3) under the cold chain, we quantified the *M.tb* burden using the Xpert MTB/RIF Cepheid kit following the manufacturer's instructions. Briefly, we carefully opened the lid of the sputum collection container and pipetted approximately 2 times the volume of the sample reagent into the sputum (2:1 dilution, Sample Reagent: sputum). We shook vigorously 15 times and incubated the sample for a total of 15 minutes at room temperature. Between 5 and 10 minutes into the incubation period, we shook vigorously 15 times. To add the sample and reagents into the cartridge, we opened the cartridge lid and then opened the sample container. Using the provided transfer pipette, we aspirated the liquefied sample close to the line on the pipette and dispensed the Sample reagent-treated sample slowly into the sample chamber of Xpert MTB/RIF cartilage to minimize the risk of aerosol formation. The cartilage lid was firmly closed and loaded into the Expert instrument for processing. The GeneXpert Instrument System generated the results from measured fluorescent signals and embedded calculation algorithms. These results were seen in the View Results window as high, medium, or trace MTB detected.

16S rRNA amplicon sequencing

DNA was extracted from samples using a sputum DNA collection, preservation, and isolation kit (Norgen Biotek Corporation, Canada; catalog no. RU46100). DNA purity and concentration were determined using both a spectrophotometer and a Qubit fluorescent-based kit. V3-V4 hypervariable region of the 16S rRNA gene was PCR amplified using 16S rRNA-specific 341F (5′ NNNNNNNNNNCCTACGGGNG GCWGCAG) and 785R (5′ NNNNNNNNNNGACTACHVGGGTATCTAAKCC) primers. All samples were tagged with unique 10 nucleotide sequences ("barcodes") incorporated into the forward primer. The PCRs included about 1 to 10 ng of DNA extract (total volume, 1 μL), 15 pmol of each forward primer, and reverse primer in 20 μL of 1× MyTaq buffer containing 1.5 units MyTaq DNA polymerase (Bioline GmbH, Luckenwalde, Germany), and 2 μL of BioStabII PCR Enhancer (Sigma-Aldrich Co). PCRs were carried out for 30 cycles. DNA concentration of amplicons of interest was assessed by gel electrophoresis. About 20 ng amplicon DNA of each sample was pooled for up to 48 samples carrying different barcodes. The amplicon pools were purified with one volume of Agencourt AMPure XP beads (Beckman Coulter, Inc., IN, USA) to remove primer dimer and other small mispriming products, followed by an additional purification on MinElute columns (Qiagen GmbH, Hilden, Germany). About 100 ng of each purified amplicon pool DNA was used to construct Illumina libraries using the Ovation Rapid DR multiplex system 1-96 (NuGEN Technologies, Inc., CA, USA). Illumina libraries (Illumina, Inc., CA, USA) were pooled and size-selected by preparative gel electrophoresis. Bacterial 16S rRNA gene amplicons were sequenced targeting the V3-V4 (300-bp

read length, paired-end protocol) region using the Illumina Miseq platform. Sequence processing and OTU classification. The raw sequences were processed to remove potential human contamination. The human genome was masked with the ProGenomes2 microbial genome database.[71] Raw reads were mapped to the human genome, discarded upon 95% identity, masked, and then filtered. Finally, we validated the human reads found by filtering out potential "human" contamination and aligned these against the NCBI nucleotide (nt) database, resulting in only top human hits. After removing human contamination, the remaining raw reads were processed using LotuS (1.62). Poisson binomial model-based read filtering was applied. OTU clustering (UPARSE) was based on sequence similarity of 97%, while SILVA was incrementally used as a database for a taxonomic assignment using a Lambda taxonomic similarity search. The taxonomic classification (genus thresholded at 95% identity) was parsed using a custom Perl script, such that unassigned taxonomic levels were assigned to the last known taxonomic level and sequentially numbered. Normalization and computation of alpha diversity measures were performed using the rarefaction tool kit (RTK 0.93.1) with default settings.

Quality control for 16S amplicon sequencing

All participants underwent sputum induction following a standard protocol to reduce sample variability. To avoid sample contamination, we used a single kit (Norgen Biotek sputum DNA isolation and preservation kit) that eliminated multiple steps of sputum processing and allowed for transportation at room temperature and inactivating microbial growth in the sample, hence preserving microbial composition. A stringent quality control check during sample collection was followed to reduce saliva and postnasal drip contamination. We also included negative controls (sputum kit with sterile water and buffer) during sample collection, DNA extraction, PCR amplification, and sequencing. Negative controls were negative for V3-V4 amplicons at PCR, and no sequences were generated.

QUANTIFICATION AND STATISTICAL ANALYSIS

Exposure and outcome variables

Our exposure variables included QFT and TB GeneXpert status. Our primary outcome variable included airway microbiome signatures.

Sample size calculation

We based on taxonomic-based human lung microbiome project (HMP) data to estimate our sample size. A conservative approximation of power to detect microbiome associations at the genus level between groups was tested using a t-test. Given n = 200 individuals in the HLM cohort, assuming an effect size of 0.8 (Cohen's d) and an alpha threshold of 0.05/30, reflecting a Bonferroni correction for the 30 main airway bacterial genera, power was approximately 80% to conclude significance for each true microbial biomarker. Clinically relevant microbial feature abundance effects that fall within the convention of a "large" effect size Cohen ($d \geq 0.8$) are frequently used as starting points for translational medicine.

Analysis plan

We summarized participant sociodemographic and clinical characteristics using proportions and used chi-squared tests to assess for differences in the distribution of these variables per three strata: Active TB, LTBI, and *M.tb*-uninfected. 16sRNA seq data: Operational taxonomical unit (OTU) counts were rarefied to the smallest retained sample size to obtain relative abundances of microbiota in each sample, accounting for read depths. Only major taxa and OTUs detected after rarefaction in at least 10% of samples were used in downstream analysis. We summarized the airway microbiome compositional differences across three strata using relative abundances (proportions) and assessed for differences in compositions across the strata using chi-squared tests. Univariate analysis was done using metadeconfoundR (version 0.2.9), and relative abundances were tested for univariate associations with clinical variables, requiring a Benjamini-Hochberg adjusted FDR of <0.1 and the absence of any clear confounders. Nonparametric tests were used for all association tests. The Wilcoxon or the Kruskal-Wallis analysis of variance was used for discrete predictors. For pairs of continuous variables, a nonparametric Spearman correlation test was used. Benjamini-Hochberg false discovery rate control (FDR) was applied in all multiple testing situations, requiring controlling the family-wise error rate at 10%. For sputum typing, we fitted a Dirichlet multinomial model on the count matrix of the genus relative abundance to classify genus abundance based on probability.[82] For microbiome network analysis, we performed Spearman's rank correlation analysis. Microbial taxa that co-occurred were considered positively associated, while mutually exclusive OTUs were negatively associated. We computed the mean co-occurrence score as the average strength of positive associations between OTUs, calculated by taking the average of the correlation coefficients. To underpin top microbiome signatures enriched in active TB versus *M.tb*-uninfected/LTBI individuals, we performed differential microbiome abundance analysis between active TB versus *M.tb*-uninfected and LTBI individuals, using EdgeR (3.14.0) and DESeq2 (1.43.1). We then projected the top enriched signatures in active TB versus *M.tb*-uninfected and LTBI individuals using a volcano plot and illustrated the top 10 enriched airway microbiome signatures in active TB versus *M.tb*-uninfected and LTBI groups. For Biomarker discovery analysis, we performed Random forest analysis in r (version 4.2.3), classified and generated microbiome signature importance plots, confusion matrices, and accuracy rates. We further conducted repeated cross-validation analyses to assess the optimal number of microbiome signatures using the Random Forest model (rf), support vector machine model (svm), and the generalized linear model (glm) models. To evaluate the performance of the models, we conducted a Receiver Operator Curve (ROC) analysis for the rf, svm, and glm models. We additionally performed Linear Discriminant Analysis Effect Size (LEfSe), a weight-based analysis method to further predict microbiome biomarkers for *M.tb* infection

status in our cohort. We used The LDA_Micro function in r (version 4.2.3) to conduct Linear Discriminant Analysis (LDA) in a microbiome context and identified differentially abundant features (OTUs) stratified by active TB versus LTBI and *M.tb*-uninfected. The identified features were ranked and filtered based on significance thresholds. We visualized the output using bar plots depicting differential features stratified by active TB versus LTBI and *M.tb*-uninfected at the genus level with LDA scores. All of the statistical details have been summarized and presented in the figure legends, figures, and results.